COO-3158-35

AN IN-SITU FIELD ION MICROSCOPE STUDY OF IRRADIATED TUNGSTEN AND TUNGSTEN ALLOYS: II. THE RECOVERY BEHAVIOR IN STAGES I and II - EXPERIMENTAL RESULTS

by

Kenneth L. Wilson and David N. Seidman

December 1974
Cornell University
Ithaca, New York
14853

Report #2347
Issued by
The Materials Science Center

DISCLAIMER

AN IN-SITU FIELD ION MICROSCOPE STUDY OF IRRADIATED TUNGSTEN AND TUNGSTEN ALLOYS: II. THE RECOVERY BEHAVIOR IN STAGES I and II - EXPERIMENTAL RESULTS*

by

Kenneth L. Wilson§‡ and David N. Seidman‡

ABSTRACT

The low temperature FIM isochronal annealing spectrum of 4 different purity levels of tungsten (resistivity ratios R of $5 \cdot 10^4$, $1.5 \cdot 10^4$, 50 and 15) irradiated in-situ with 30keV W^+ ions to a dose of $5 \cdot 10^{12}$ ion cm^{-2} at 18K consisted of distinct recovery peaks at ∿38, 50, 65 and 80K with a small amount of recovery observed up to 120K. The spectra for these 4 different R value specimens were essentially identical between 18 and 120K. A fifth group of W specimens with $R \simeq 5$ began to exhibit some deviations from the standard spectrum. This result indicates that the distribution of self-interstitial atoms (SIA's) produced by the ion irradiations in the W FIM tips was such that the SIA-SIA reaction dominated the recovery behavior. The isochronal peak width at half-maximum for the 38K long-range SIA migration peak and the Stage II peaks in pure W were shown to be approximately equal to the value predicted by a diffusion model. The isochronal recovery spectra for tungsten-0.5 at.% and 3 at.% rhenium alloys were radically different from the isochronal recovery spectra of pure W. For both W-(Re) alloys the amount of recovery for the long-range migration peak was suppressed and for the 3 at.% Re alloy it was almost eliminated. This result constitutes evidence for the formation

---

* Research supported by the United States Atomic Energy Commission. Additional support was received from the National Science Foundation through the use of the technical facilities of the Materials Science Center at Cornell University.

§ Now at: Sandia Laboratories, Livermore, California 94550.

‡ Cornell University, Bard Hall, Department of Materials Science and Engineering and the Materials Science Center, Ithaca, New York 14853.

of tightly bound immobile SIA-Re complexes during the long-range migration sub-stage at 38K which suppress the SIA-SIA reaction. High-purity W ($R=5\cdot10^4$) doped with 50-100 appm carbon showed a 20% reduction in the amount of recovery observed for the long-range migration peak at 38K. The substage II_A peak at ∿50K grew at the expense of the 38K peak. This result constitutes evidence for the formation of SIA-carbon atom complexes during the long-range migration peak at ∿38K. An analysis of the SIA contrast patterns detected in the isochronal anneals indicated that some form of SIA clustering must have occured below 120K (Stage II). Preliminary high dose ($5\cdot10^{13}$ W^+ ion cm^{-2}) experiments also exhibited a suppression of the 38K peak and indicated that more SIA clustering was occuring than in the low dose ($5\cdot10^{12}$ ion cm^{-2}) experiments.

I. INTRODUCTION

In Part I[1] it was shown that the volume change of migration (Δv_{1i}^m) of the Stage I self-interstitial atom (SIA) is $<0.02\Omega_a$ and that the long-range migration peak for the SIA occurs below 45K (the maximum in this peak occurs at ~38K). In addition, the 100K irradiation experiment of Scanlan et al.[2] demonstrated that the early Stage II field ion microscope (FIM) recovery peaks (~45 to 120K) were <u>not</u> higher temperature recovery peaks shifted downward in temperature (T) by a $p\Delta v_{1i}^m$ effect [where p is the pressure due to the electric field (E)]. Furthermore, the FIM isochronal annealing experiments of Scanlan et al.[2] and the present work demonstrate that these early Stage II isochronal recovery peaks in W involve the motion of some form of the SIA. A number of the isochronal peaks observed by the FIM technique are quite similar to those detected via electrical resistivity measurements (see Dausinger et al.[3] for a comparison of the data from the two techniques). Hence, the experiments reported in this paper were aimed at trying to answer the question of whether this SIA migration was an intrinsic or an extrinsic phenomenon or involved both mechanisms.

Detrapping of SIA's from extrinsic impurity atoms has been studied in detail in a number of face-centered cubic (F.C.C.) metals by electrical resistivity measurements.[4,5,6,7] The FIM isochronal warming technique has been employed recently by Wei and Seidman[8] to measure the dissociation energy of SIA's from gold atoms in an ion irradiated Pt-0.62at.%Au alloy in the temperature regime (~90K) of substage II_c.[9] The body-centered cubic (B.C.C.) metals such as tantalum[10,11,12] have exhibited large impurity atom effects on the isochronal annealing behavior. With respect to the FIM situation Seidman and Lie[13] studied analytically the problem of SIA diffusion in an FIM tip containing a uniform distribution* of impurity atoms. The results of their analysis predicted an impurity

---

* This model also assumed a uniform initial distribution of SIA's and neglected SIA-SIA cluster reactions. In view of the present work and a little hindsight it is clear that these mathematical assumptions are not strictly valid.

atom effect which was a strong function of the concentration of impurity atoms and only a weak function of the binding energy of the SIA to the impurity atom. In brief, their analysis predicted that the Stage I long-range migration recovery peak was diminished by the addition of impurity atoms and that there was a flux of SIA's in Stage II which occured when the impurity atoms released the SIA's or the SIA-impurity atom complexes became mobile.

Alternatively there is also evidence for intrinsic phenomena in Stage II. Evidence for SIA cluster growth has been found by Bourret[14] for Ni and by Urban and Seeger[15] for Pb via transmission electron microscopy. Also diffuse x-ray scattering studies have given evidence for SIA cluster growth in both Al[16] and Cu.[17] In addition, both Afman[18] and Moser[19] have suggested that there may be additional intrinsic defects present in irradiated B.C.C. metals. They proposed an extended interstitial that resembles a one-dimensional dissociated edge dislocation. From the above brief literature survey one can see that both intrinsic and extrinsic mechanisms may be important in explaining the FIM observations in Stages I and II of W^+ ion irradiated tungsten.

In this paper (Part II of a four part series) the results of a detailed investigation of the effects of impurity atoms in "pure" tungsten, as well as tungsten-(rhenium) and tungsten-(carbon) alloys, on the isochronal annealing spectrum of FIM specimens which have been irradiated <u>in-situ</u> with 30keV W^+ ions to a dose of $5 \cdot 10^{12}$ ion cm^{-2} are reported. The essentially identical results obtained from four different purity levels of tungsten (resistivity ratios R of $5 \cdot 10^4$, $1.5 \cdot 10^4$, 50 and 15) show that SIA-SIA reactions dominated the recovery behavior. A fifth group of tungsten specimens with $R \simeq 5$ began to exhibit deviations from the spectra obtained for the higher purity tungsten specimens and the effects of impurity atoms became even more pronounced in the tungsten-(carbon) and tungsten-(rhenium) alloys. These results provide further proof that the distribution of SIA's around the depleted zones created by the 30keV W^+ ions was such that the SIA-SIA reaction

was favored in the "pure" tungsten specimens ($R \geq 15$) and that for $R \simeq 5$ the SIA-impurity atom reaction began to become important. The recovery behavior of the carbon doped tungsten and tungsten-(rhenium) alloys demonstrates that both SIA-carbon atom and SIA-rhenium atom complexes are stable in tungsten. Additional direct evidence was presented for SIA clustering from high dose ($5 \cdot 10^{13}$ ion cm^{-2}) experiments where both isochronal annealing and post-anneal field evaporation experiments were employed to demonstrate the existence of SIA clusters.

2. ADDITIONAL EXPERIMENTAL DETAILS

2.1. Preparation of FIM tips

For the polycrystalline specimens employed in these studies the ac dipping method was employed to make an FIM specimen. The dc drop-off technique used for the single crystal specimens has been described in Part I.[1] In the ac dipping method a 0.1mm diameter wire was immersed vertically to a depth of 3mm in a 1N NaOH aqueous solution and a 4 to 5Vac potential was applied between the wire specimen and a stainless steel electrode. The wire quickly developed a tapered tip and the electropolishing was terminated when ∿2mm of metal had been removed from its end. A specimen produced by the ac dipping technique usually imaged at 3 to 4kV in the FIM. This method produced good specimens from polycrystalline drawn wires, but met with only minimal success for the zone-refined single crystals. Possibly, some preferential crystallographic etching hampered tip development in the case of the single crystals.

2.2. Preparation of tungsten-carbon alloys

Both four-pass zone-refined and Westinghouse annealed tungsten wire were doped with carbon* by a quenching technique similar to the one described by

---

* Carbon is an interstitial impurity atom in tungsten with an extremely small solid solubility in tungsten. The solubility of carbon in tungsten is believed to be $\lesssim 0.5$ at.% at 2475°C.[21]

Krautz et al..[20] The single crystal tungsten specimen which was quenched was first electropolished to a diameter of 0.2mm; next, it was suspended vertically in a vacuum chamber which was backfilled to a partial pressure of $1 \cdot 10^{-4}$ torr methane. The electrical and thermal contacts to the specimen were made by clamping the specimen at its top end and immersing the bottom end in a liquid ternary eutectic of gallium, indium and tin which has a melting point of 10°C (United Mineral and Chemical Corp., alloy UG-1). The specimen was resistively heated to 1500°C for a period of 4h and then radiation quenched. An annealed Westinghouse tungsten wire of 0.125mm diameter was quenched in a similar manner after being equilibrated for 4h at 2000°C in 10^{-4} torr methane.

In the case of the four-pass zone-refined tungsten specimen the value of R was $\triangleq 250$ after the quench. The only available value for the resistivity of a C atom in solid solution in W is $3.85 \cdot 10^{-6} \Omega cm(at.\%)^{-1}$[20]; thus, on the basis of this number the single crystal contained $\sim$50appm carbon. The C concentration in solid solution in the polycrystalline wire could not be established quantitatively. The wire was quenched from a higher temperature at a faster quenching rate* than the single crystal, but the grain boundaries in the wire specimen certainly served as a good internal sink for the rapidly diffusing C** atoms. The end result was that the polycrystalline wire exhibited extreme brittleness after this C doping treatment.

3. MATERIALS EMPLOYED

A total of five different purity levels of pure tungsten were investigated; they were:

(1) Four-pass zone-refined single crystals ($R=5 \cdot 10^4$),

---

* The quenching rate of a wire due to radiation cooling is inversely proportional to its diameter.

** The diffusivity of a carbon atom in a tungsten lattice is given[22] by $(3.4 \cdot 10^{-3}\ cm^2 sec^{-1}) \exp(-1.6eV/kT)$.

(2) One-pass zone-refined single crystals (R=1.5·10^4),

(3) Westinghouse polycrystalline wire annealed at 2400°C for one hour in a vacuum system which was at $\lesssim$1·10^{-5} torr (R=50),

(4) Materials Research Corporation (MRC) VP grade wire (R=15),

(5) Westinghouse polycrystalline wire in the as-received state (R=5).

The zone-refined single crystals were grown from both 1.03 and 1.55mm diameter rods of commercial purity tungsten.

Two standard physical measurements were employed to determine the purity of these specimens. The first technique employed was chemical analysis in the form of spark source mass spectrometry (SSMS).* This technique gave us the chemical composition of the metalic elements present in the specimen; however, SMSS does not distinguish between impurity atoms which were in solid solution and those which were in precipitates. Interstitial impurity atom concentrations were measured by standard quantitative analysis (e.g., the inert gas fusion technique for C), but again there was no determination of the location of the impurity element.

The second measurement of specimen purity is the resistivity ratio R [$R=\rho_{273K}/\rho_{4.2K}$]** which has also been used in Part I.[1] The value of $\rho_{4.2K}$ is sensistive to the total impurity atom concentration in solid solution.[23] Unfortunately, R also does not provide any information on which impurity atoms are in solid solution. The tabulated values[2] of the specific resistivities of impurity atoms in tungsten indicate that a reasonable value to use is $\simeq$1·10$^{-6}\Omega$cm(at.%)$^{-1}$, although Dausinger et al.[3] have employed a value as low as 0.2·10$^{-6}\Omega$cm(at.%)$^{-1}$ for molybdenum in tungsten.

Tables 1 and 2 summarize the results of the chemical analyses and the R data for the different specimens employed in this study. The value $R\cong$5·10^4 corres-

---

* The SSMS technique is only good to within an order of magnitude unless reference standards are used for each specific element in question. Reference standards were not available for tungsten when the analyses of our specimens were performed.

** The value of ρ_{273K} has been taken to be equal to 4.95·10$^{-6}\Omega$cm.[24]

ponds to at most a few appm of impurity atoms, while $R \gtrsim 5$ corresponds to an impurity atom concentration of $\lesssim 10^4$ appm (based on $1 \cdot 10^{-6}$ Ωcm(at.%)$^{-1}$ as the specific resistivity of an impurity atom). It is clear from a comparison of Tables 1 and 2 that the chemical analyses* and R data are not in agreement. This is indicative of the fact that the concentration of impurity atoms in solid solution must have been quite different from the total impurity atom concentration in each specimen. The two W-(Re) alloys studied contained 0.5 and 3at.% Re respectively. The results of the SSMS of these two alloys are also given in Table 1. The R values for the W-(Re) alloys are shown in Table 2 and it is seen that these values are consistent with our interpretation that $R=5 \cdot 10^4$ corresponds to $\sim 10^{-6}$ at.fr. impurities and $R \gtrsim 5$ corresponds to $\sim 10^4$ appm impurities.

4. RESULTS**

4.1. Isochronal recovery behavior of the different grades of tungsten.

The isochronal recovery spectra for the one-pass zone-refined ($R=1.5 \cdot 10^3$), Westinghouse annealed ($R=50$) and the MRC VP grade tungsten ($R=15$) are presented in Figs. 1 to 3 respectively. The spectrum for the four-pass zone-refined ($R=5 \cdot 10^4$) has been previously presented [see Fig. 2(A) of Part I]. The histograms show the fraction of SIA defects per 5K interval as a function of T in the range 18 to

---

* For example the lower limit on the total impurity content suggested by the SSMS of the four-pass zone-refined specimen is $\sim$14 appm while the R values suggest $\sim$1 to 3 appm.

** The histograms exhibited in this section were constructed from the superposition of several runs, with a maximum of three irradiations performed on each tip. From 100 to 1000Å of metal was removed between each irradiation to increase the bluntness of the tip. In order to ascertain the effect of re-irradiating a given specimen two runs were made on the same crystal with only 5Å removed between the irradiations. No large changes were found in the isochronal annealing spectra indicating that the depleted-zone distribution and density did not play a major role in the observed recovery behavior after a standard dose of $5 \cdot 10^{12}$ W^+ ion cm^{-2} (for the effect of dose se Section 4.6). Table 3 summarizes the relevant data for all the isochronal anneals performed.

120K for specimens which were irradiated with 30keV W^+ ions at 18K in the absence of E. These four different grades of W displayed remarkably similar annealing spectra. The 38K long-range migration peak was the dominant feature in all four cases. Three distinct recovery peaks were found at ∿50, 60 and 80K and an ill-defined tail which might contain additional peaks at 95 and 110K was also observed.

The peaks were spaced closely enough so that there was considerable* overlap. In order to obtain a more accurate picture of the amount of recovery per peak the results were re-analyzed with a 15K increment; each increment was centered about a recovery peak. Figure 4 shows the percent of recovery per 15K interval as a function of T. Note that only the Stage I long-migration peak at 38K and the Stage II peaks at 50, 65 and 80K are shown. This plot demonstrates the uniformity of the recovery in these four different grades of tungsten. The quantity R was varied from $5 \cdot 10^4$ to 15 yet only minor variations were seen in the FIM isochronal recovery spectra.

The fifth grade of tungsten studied was Westinghouse wire in the as-received state (R=5). The isochronal spectrum (see Fig. 5) lacked the sharp peak structure found in the purer specimens, but the dominant 38K peak was still present. Hence, the value of R for pure tungsten was varied by a factor of 10^4 and the annealing spectrum was just beginning to show some changes. These experiments, in conjunction with the isochronal recovery experiments on the W-(Re) and W-(C) alloys described in Sections 4.3 and 4.4, lead us to the conclusion that for the unalloyed tungsten specimens the SIA's only interacted weakly with the impurity atoms in the FIM tips and that SIA-SIA interactions dominated the recovery behavior. This situation was a result of the distribution of SIA's around the depleted zones created by the 30keV W^+ ions. The heavy metal ion irradiation produced an initial

---

* The scatter in the data taken from different runs with slightly different warming rates and tip radii also contributed to the broadening of these peaks.

state of damage which consisted of a cloud of SIA's surrounding each depleted zone[26] thus the distribution of SIA's was highly non-random with respect to the distribution of impurity atoms in the tip volume and hence favored the SIA-SIA reaction.

4.2. The experimental isochronal annealing width of the Stage I long-range migration peak

In order to study the experimental width of the Stage I long-range migration peak the data for the 38K peak of the annealed Westinghouse tungsten specimens were analyzed employing a 2K temperature interval. This particular type of specimen was chosen for the analysis because all the data were obtained from three different irradiations on the same specimen. The tip radius varied by only 20Å (see Table 3) between the first and the last irradiation. The possible broadening effect due to the superposition of different runs on tips of different radii was thereby minimized.* Since the 38K and 50K peaks tended to overlap the termination of the long-range migration peak could not be determined unambiguously; hence, it was set at 42K. The 74 SIA events detected below 42K in the spectrum of the annealed Westinghouse tungsten are displayed in Fig. 6. Superimposed on this peak is the analytical curve of Scanlan et al.[2] for the flux of single thermally activated SIA's diffusing across the surface of a spherical FIM tip. The dimensionless parameter Γ was set equal to 10^{16} and the curve was positioned so the T_m coincided with the experimental value. The areas under the theoretical curve and the experimental histogram were set equal to each other. While the fit was not perfect the experimental histogram did approach the theoretical width at half-

---

* The diffusion model of Scanlan et al.[2] predicted a peak temperature given by the expression:

$$T_m \cong \frac{\Delta h_{1i}^m}{k}[\ln\Gamma - 2\ln\ln\Gamma]^{-1},$$

where $\Gamma = \pi^2 D_{1i}^{\circ} \Delta h_{1i}^m / R^2 \alpha k$, R is the tip radius and α is the isochronal warming rate. Any variation in R or α would tend to shift T_m slightly from run-to-run.

maximum of 4K.* The leading edge of the experimental histogram extended to lower temperatures than the model predicted. This premature flux can be attributed to SIA's positioned originally only a few atom layers below the surface. A calculation by Beeler[27] has shown that the value of Δh^m is significantly less than the bulk value for the first few layers below an external surface. Hence, the near surface SIA's would have become mobile at a lower T than the bulk SIA's.

The Stage II recovery peaks also possessed widths at half-maximum that were in good agreement with the model calculation. However, this experiment could not resolve peaks that were separated by $\lesssim$5K. Therefore, each of the Stage II peaks may have been caused by more than one single thermally-activated process. Because of the peak broadening introduced by the superposition of several runs it was felt that a 5K temperature interval was sufficient to display the main features of the annealing spectra. Only in the case just discussed did the 2K interval provide additional information.

4.3. The isochronal annealing spectra of tungsten-rhenium alloys

The five grades of W used for the studies presented in Section 4.1 each contained less than 10appm Re (see Table 1). The isochronal annealing spectra of the irradiated W-0.5at.% Re ($5 \cdot 10^3$appm) and W-3at.% Re ($3 \cdot 10^4$appm) alloys are presented in Figs. 7(A) and 7 (B). Both of these histograms display the number of defects per 5K interval as a function of T.

In the case of the W-0.5at.% Re alloy the long-range migration peak temperature was between 30 and 35K instead of at 38K as in the case of the undoped W specimens. This shift is easily explained if one considers that only the SIA's close to the surface could reach the surface without being trapped by Re atoms.

---

* The analytical treatment of Scanlan et al.[2] predicted that the width at half-maximum is given by $\sim T_m/10$.

These SIA's would constitute the early part of the flux because of the short diffusion distance to the surface. This downward shift in T_m with increasing impurity atom concentration has been predicted by the Seidman and Lie treatment of this diffusion problem (see Fig. 6 in reference 13). The substage II_A peak at 50K has now become the dominant peak, while the 60 and 80K peaks have almost vanished. In addition, there is an increase in the amount of recovery for the peaks at 95 and 110K.

The W-3at.% Re alloy showed almost no recovery over the entire range from 18 to 120K. The recovery peak at 110K was the largest one, but it contained only three SIA's after a total of six recovery experiments. Thus, for both of these alloys there is strong evidence that the SIA's formed SIA-Re atom complexes in Stage I. In the case of the W-3at.% Re alloy the fraction of the Stage I SIA's trapped was appreciable since the 38K peak was essentially eliminated.* It should be noted the recovery behavior in Stage II has also been radically changed; this latter result indicates that the SIA-SIA reactions have almost been completely suppressed and that the SIA-Re atom complexes have a significant dissociation energy (>0.27eV). Additional experiments at higher temperatures are in progress (Nielsen and Seidman) to detect the recovery peak caused by the release of SIA's from Re atoms and perhaps di-Re atoms.

4.4. The isochronal annealing spectra of tungsten-carbon alloys

Figure 8 exhibits the isochronal annealing spectrum of the four-pass zone-refined W with ∿50appm of C in solid solution. The substage II_A peak at ∿50K has grown in size at the expense of the long-range migration peak at ∿38K. The isochronal annealing spectrum of the Westinghouse W doped with C (Fig. 9)

---

* This suppression of the SIA long-range migration recovery peak has also been observed for a number of f.c.c. cubic alloys (e.g., see Sosin and Neely[28], Sosin[4] and Schilling et al.[29]).

also showed this increase of the substage II_A peak at the expense of the long-range migration peak. Figure 10 shows the data from these two spectra re-analyzed with a 15K temperature interval. A comparison of these spectra with the spectra for undoped W summarized in Fig. 4 makes it obvious that the introduction of C into solid solution has changed the recovery behavior of W. Quantitatively we can state that the 38K peak was diminished by ∿20% when the C level in the four-pass zone-refined W ($R=5\cdot10^4$) was increased by a factor of ∿200 over its concentration in the undoped single crystals. This experiment also provides direct evidence for the formation of SIA-carbon atom complexes during the long-range migration peak and in this case the subsequent release of the SIA's from the complexes at ∿50K.

4.5. SIA contrast patterns detected during isochronal anneals

The primary contrast pattern produced by the flux of SIA's during the isochronal warming experiments, was a single extra atom spot.* Figure 11 shows several typical examples of this contrast pattern from different regions of a tungsten surface (also see Fig. 6 in Scanlan et al.[2] and Fig. 4 in Robinson et al.[30]). Amongst the 1062 SIA events observed in the isochronal annealing experiments (see Section 4.1) 91.25% exhibited this simple contrast pattern. The remaining SIA events were multiple spot contrast patterns** similar to the four examples shown in Fig. 12. The double-spot contrast pattern was observed in 6.68% of the total number of events, while triple-spot contrast patterns occurred in 1.22% of the observed contrast patterns. Clusters of four or more extra spots constituted only 0.85% of the 1062 events observed.

---

* This contrast pattern has also been referred to as an extra "bright" spot by a number of authors.

** Multiple spot contrast patterns were considered as single SIA events in the construction of the isochronal annealing histograms, hence the use of the term defects in labeling the ordinates.

The single-spot contrast effect could have arisen from an atom on the surface (an adatom created by the total relaxation of an SIA at the surface) or by a surface or a subsurface atom that was displaced upward as a result of an SIA lying several atomic layers below the specimen's surface (Seidman and Lie[31]). Figure 1 in Robinson et al.[30] illustrates these possibilities on the (011) terraces. On the experimental side it is extremely difficult to distinguish between these two mechanisms. The single-spot contrast effect resembles the contrast effect due to adatoms that had been vapor deposited[32] onto an FIM specimen and also to the last atom on a plane that had been pulse field evaporated[33]; but this visual similarity of the contrast effects was not enough to make a distinction between the two mechanisms. While the single-spot contrast effect has been assumed to be the result of a single SIA at or near the surface the double-spot contrast pattern may have had two distinct origins. First, the contrast model of Seidman and Lie[31] predicted that for certain orientations the <110> split SIA can produce a double-spot contrast effect at the surface; this model requires that the SIA retains its identity as a subsurface defect. Second, the double-spot contrast pattern could indicate the arrival of a di-SIA complex at the surface. Figure 13 exhibits the fraction of defects per 5K temperature interval as function of T for only the double-spot contrast effects found in the isochronal anneals of all five grades of undoped tungsten. It can be seen that the double-spot contrast effects occurred over the entire range of T in which single-spot contrast effects were observed. The coexistence of single and double-spot contrast effects in the 38K long-range migration peak tends to indicate that both contrast effects had the same origin (i.e., the single SIA). Therefore, a reasonable conclusion is that at least some of the SIA contrast effects were caused by the strain field of a subsurface SIA. Whether this mechanism was the only one that was operative cannot be ascertained at present.

Contrast patterns with three or more spots (see the pairs of micrographs E and F and G and H in Fig. 12) were much larger than the predicted strain field contrast effect patterns of Seidman and Lie[31] for the single SIA. While these events were only a small portion (∿2%) of the total number of defects, their appearance indicated that some form of SIA clustering must have occured within the FIM specimen during the isochronal anneals. Because of the small number of multiple contrast patterns it was not clear if their migration was possibly assisted by a large negative $|p|\Delta v_{ic}^{m}$ effect; where Δv_{ic}^{m} is the volume change of migration of the SIA cluster. With respect to the latter point the 100K irradiation experiment of Scanlan et al.[2] showed that the single-spot peak structure observed below 100K in the isochronal anneals was <u>not</u> assisted by the electric field. Their experiment did not rule out a $p\Delta v_{ic}^{m}$ effect for the SIA clusters. In fact, the three SIA events detected in the isochronal recovery below T_i=100K were multiple-spot contrast effects.

The 50K irradiations described in Part I showed an increase in all forms of multiple-spot contrast patterns over the 18K irradiations. Double-spot contrast patterns constituted 10.60%, triple 6.38% and 5.31% larger clusters (greater than triple-spot contrast patterns) were observed. The major implication of this result is that clustering must have occured primarily between SIA's which were ejected from a single depleted zone; since, in the case of the 50K irradiations the SIA's were highly mobile and hence able to reach an internal sink or the surface before the next depleted zone was created. This conclusion is reasonable because the local SIA concentration in the immediate vicinity of a newly created depleted zone was estimated to be $\sim 10^{-3}$ at.fr. or greater* for the case of an 18K irradiation.

---

* This concentration is calculated by assuming that $\sim 10^{2}$ SIA are contained within a sphere of ∿100Å radius (Beavan et al.[26]) around each depleted zone.

In the case of the 50K irradiations it is possible to have even a higher local SIA concentration since the mean range of an RCS is temperature dependent[34], and hence the SIA's may be confined to an even smaller volume of metal than in the case of the 18K irradiation. A high local concentration of SIA's implies a small number of jumps for one SIA to reach another SIA, and hence there is a high probability of SIA cluster formation. It is clear that if the concentration of SIA's was assumed to be uniform throughout the volume of the FIM specimen then the probability of SIA cluster formation would be strongly reduced.

4.6. The dose dependence of the isochronal annealing spectrum

A few preliminary experiments were conducted to determine the dose dependence of the isochronal annealing spectrum. Three runs were made on Westinghouse annealed tungsten polycrystalline wire irradiated at 18K to a dose of $5 \cdot 10^{13}$ W^{+}ions cm^{-2}. This dose was a factor of ten greater than the standard irradiation dose. Figure 14 exhibits the isochronal recovery spectrum. The long-range SIA migration peak at ∿38K has diminished in size, while the substage II_A peak at ∿50K has grown. In addition, the SIA flux out of the tip was extremely anisotropic. Almost no recovery was observed on the half of the tip exposed to the ion beam. This phenomenon was most likely caused by internal SIA recovery at depleted zones or by the formation of immobile SIA clusters. Five of the 62 SIA events (or 8%) in the isochronal anneals were multiple contrast patterns with more than three spots. This fact indicates that extensive SIA clustering had indeed occurred in Stage I. Furthermore, this decrease in the amount of recovery of the SIA long-range migration peak in Stage I with increasing dose has also been found for the long-range migration peak in a number of pure f.c.c. metals irradiated with fast neutrons (1MeV), α-particles (5MeV), and electrons (3MeV) (e.g., see Figs. 32 and 33 in Schilling et al.[29] for data on Cu and Al). Thus, this dose-dependence experiment is also consistent with the long-range migration peak being at ∿38K.

A post-anneal peel was performed on an MRC wire that had been irradiated to $5 \cdot 10^{13}$ W^+ ion cm^{-2} at 18K, annealed to 120K, and then recooled to 18K. The remnants of numerous depleted zones were found on the beam side of the tip. This particular specimen was a bi-crystal, with a grain boundary running almost parallel to the beam direction. Three defects with large strain fields were found among 66,500 atomic sites examined in the (111) region on the beam side (crystal I). The (111) region in crystal II (on the side of the tip away from the beam) had zero defects in 61,000 atomic sites studied. A (114) plane in crystal II located between the two (111) regions had one SIA-like contrast pattern in 6,000 atoms. Several other bright-spot SIA contrast effects were observed inside depleted zones, but were not included in these statistics.

This preliminary post-anneal peel on a specimen which had been irradiated to a high dose indicated that the SIA defect concentration was $\sim 5 \cdot 10^{-5}$ to $1 \cdot 10^{-4}$ at. fr. in the volume of the tip on the beam side and $\leq 1 \cdot 10^{-5}$ at. fr. in the other half of the tip. The defects themselves exhibited large strain fields and the field evaporation behavior of the plane several atomic layers above the observed extra bright spot was altered dramatically. Figure 15 shows the appearance of one of these defects on a (334) plane. The size of these defects indicated that they were most likely SIA clusters. However, no detailed results on the exact nature of the defects can be made without further analytical studies of SIA clusters and their behavior near free surfaces. The low concentration of SIA defects found in pulse field evaporation experiments hinders any classification that could lead to an empirical technique for cluster size determination. But, we emphasize the fact that this post-anneal peel is also indicative of SIA cluster formation in Stage I and subsequent SIA cluster growth in Stage II.

4.7. Control experiments

Six control runs were made during the course of the isochronal annealing experiments. Three of the specimens were simply annealed from 18 to 120K without being irradiated, while the other three specimens had been irradiated but had flashed* during the post-irradiation peel prior to the isochronal anneal.

One contrast pattern similar to an SIA was observed in the first control run on an unirradiated specimen. No SIA contrasts were observed in any of the subsequent control runs. This single contrast effect in these controls may have been caused by a gas impurity atom that had been adsorbed on the surface. The high electric field required for field ionization of helium kept impurity adsorption to a minimum.[35] In one of the control runs, the specimen was exposed to the ion accelerator (at $\sim 10^{-5}$ torr argon gauge pressure) though the differential pumping system for ~30 minutes. No SIA contrast effects were observed in the subsequent control anneal from 18 to 120K. If these six specimens had been irradiated at 18K and annealed normally there would have been ~150 SIA events detected.** Therefore an upper maximum to the gas impurity contamination effect was $\leq 0.7\%$ for the isochronal anneals. This background is insignificant with respect to the SIA flux observed in the isochronal anneals reported.

5. MAJOR EXPERIMENTAL RESULTS

The principle experimental results are summarized as follows:

(1) The low temperature isochronal annealing spectrum of pure tungsten ($R=5\cdot10^4$), irradiated <u>in-situ</u> with 30keV W^+ ions to a standard dose of $5\cdot10^{12}$ cm^{-2} at 18K was

---

* Flashing is a common mode of tip failure whereby a shell of material is expelled from the surface. The tip is still imagable at a higher voltage, but the SIA's have been swept out (see Wilkes et al.[36] and Loberg[37] for more details on tip failure).

** This number was calculated for 30keV W^+ ions for a dose of $5\cdot10^{12}$ ions cm^{-2} assuming approximately one observable SIA per incident ion. This number is borne out by our experimental results.

shown to consist of a series of distinct recovery peaks at ∿38, 50, 65 and 80K with a small amount of additional recovery observed up to 120K. We had previously identified the 38K peak as the SIA long-range migration substage. The remaining peaks were classified as substages of Stage II. Thus, Stage II of irradiated tungsten begins at ∿45K and not at ∿100K as had been suggested by earlier investigators.

(2) The isochronal annealing spectrum of pure tungsten observed by FIM between 18 and 120K was insensitive to R for values between 15 and $5 \cdot 10^4$. Specimens with $R \simeq 5$ began to show some deviation from the standard spectrum. This result indicates that the distribution of SIA's produced by the 30keV W^+ ion irradiations in the FIM tips was such that the SIA's only interacted weakly with the impurity atoms and that the SIA-SIA reaction dominated the recovery behavior.

(3) The isochronal peak width at half-maximum for the 38K long-range SIA migration peak in pure tungsten was shown to be approximately equal to the value predicted by an analytical expression developed by Scanlan et al.[2] based on a single thermally-activated diffusion model. The Stage II peaks also obeyed this diffusion model prediction.

(4) The isochronal annealing spectra for tungsten-0.5 at.% and 3 at.% rhenium alloys were radically different from the isochronal recovery spectra of pure tungsten. For both tungsten-(rhenium) alloys the amount of recovery for the long-range migration peak at ∿38K was suppressed and in the case of the 3 at.% Re alloy it was almost eliminated. This result constitutes strong evidence for the formation of immobile tightly bound SIA-rhenium complexes during the long-range migration substage at 38K which suppress the SIA-SIA reaction.

(5) Tungsten doped with ∿50-100 appm carbon showed a 20% reduction in the amount of recovery observed for the long-range migration peak at 38K in undoped tungsten. The substage II_A peak at ∿50K grew at the expense of the 38K peak. This result constitutes evidence for the formation of SIA-carbon atom complexes during the

long-range migration peak at ∿38K. In this case the concentration of carbon was not large enough to completely suppress the SIA-SIA reaction.

(6) The SIA contrast patterns detected in the isochronal anneals consisted primarily of single extra spots. However, the small number of large multiple spots indicated that some form of SIA clustering must have occurred below 120K in Stage II during the isochronal anneal. The increase of multiple-spot contrast patterns in the isochronal anneals following a 50K irradiation can be understood in terms of a decreased focused collision replacement sequence range which lead to a higher local concentration of SIA's in the vicinity of each depleted zone and hence a greater concentration of SIA-SIA clusters.

(7) Preliminary high dose ($5 \cdot 10^{13}$ ion cm^{-2}) experiments also exhibited a suppression of the 38K peak and indicated that more SIA clustering was occurring than in the low dose ($5 \cdot 10^{12}$ ion cm^{-2}) experiments. The evidence for SIA clustering came from both the isochronal annealing experiment and a post-anneal pulse field evaporation; although an exact cluster size determination was not possible.

ACKNOWLEDGEMENTS

The authors wish to thank Mr. B.F. Addis for his help in the preparation of the zone-refined single crystals of tungsten and the carbon doped tungsten specimens, Mr. C. Nielsen for measuring the resistivity ratios of the tungsten-(rhenium) alloys, Mrs. K. Pratt for her aid in scanning ciné film and Mr. R. Whitmarsh for his technical assistance.

REFERENCES

1. K.L. Wilson and D.N. Seidman, Cornell University Materials Science Center Report No. 2346 (1974).
2. R.M. Scanlan, D.L. Styris and D.N. Seidman, Phil. Mag. 23, 1439 (1971); R.M. Scanlan, D.L. Styris and D.N. Seidman, Phil. Mag. 23, 1459 (1971).
3. F. Dausinger, H. Schultz, K. Bönig, G. Vogl, Tagungstortrag, Physikertagung in Freudenstadt, April (1964).
4. A. Sosin, in Lattice Defects and Their Interactions, edited by R.R. Hasiguti, pp.235-66. Gordon and Breach (1968).
5. For example, see T.H. Blewitt, R.R. Coltman, C.E. Klabunde and T.S. Noggle, J. Appl. Phys. 28, 639 (1957); D.G. Martin, Phil. Mag. 6, 839 (1961); A. Sosin and H. Neely, Phys. Rev. 127, 1465 (1962); A.Sosin and L.H. Rachal, Phys. Rev. 130, 2238 (1963); and A. Sosin, J. Phys. Soc. Japan 18, Suppl. III, 227 (1963).
6. M. Doyama, J.S. Koehler, Y.M. Lwin, E.A. Ryan and D.G. Shaw, Phys. Rev. B4, 281 (1971).
7. F. Dworschak, A. Kraut, K. Sonnenberg and H. Wollenberg, Rad. Effects 19, 119 (1973).
8. C-Y. Wei, M.S. Thesis, Cornell University (1975); C-Y. Wei and D.N. Seidman, Cornell University Materials Science Center Report No. 2392 (1975).
9. W. Schilling, K.Sonnenberg and H.J. Dibbert, Rad. Effects 16, 57 (1972).
10. K. Faber, H. Schultz and F. Walz in Reinstoffe in Wissenschaft und Technik, 4, pp.54-55. Ackademie-Verlag (1972); K. Faber, J. Schweikhardt and H. Schultz, Scripta Met. 8, 713 (1974).
11. G. Burger, K. Isebeck, R. Kerler, J. Vökl, H. Wenzl, H.-H. Kulhmann and H. Schultz, Phys. Letters, 20, 470 and 472 (1966).
12. H. Hemmerich, D. Meissner, H. Schultz and F. Walz, in preprints (only) of Vacancies and Interstitials in Metals, Vol. 2 (Zentralbibliothek der Keinforschungsanglage Jülich GmbH) pp. 724-732 (1968).
13. D.N. Seidman, J. Phys. F: Metal Phys. 3, 393 (1973).
14. A. Bourret, Phys. Stat. Sol. (a) 4, 813 (1971).
15. K. Urban and A. Seeger, Phil. Mag. 30, 1395 (1974).
16. P. Ehrhart and W. Schilling, Phys. Rev. B8, 2604 (1973).
17. P. Ehrhart and V. Schlagheck, KFA Jülich Report (1974).
18. H.B. Afman, in Defects in Refractory Metals, edited by R. deBatist, J. Nihoul and L. Staals, pp. 19-20. S.C.K./C.E.N., Mol (1972).
19. P. Moser, in Defects in Refractory Metals, edited by R. deBatist, J. Nihoul and L. Staals, pp. 65-67. S.C.K./C.E.N., Mol (1972).

20. E. Krautz, H.-H. Kuhlmann and H. Schultz, Z. Metallk. 59, 133 (1968).

21. M. Hansen and K. Anderko, Constitution of Binary Alloys; p. 392. McGraw-Hill (1958); E. Fromm and H. Jehn, Met. Trans. 3, 1685 (1972).

22. A. Shepella, Ph.D. Thesis, Cornell University (1970).

23. K.H. Berthel, Phys. Stat. Sol. 5, 159 (1964).

24. V.Y. Startsev, N.V. Volkenshteyn and G.A. Nikitina, Fiz. Metal. Metalloved. 26, 261 (1968).

25. M. Drechsler and P. Wolf in Proc. 4th Int. Cong. Electron Microscopy, Vol. 1, pp.835. Springer-Verlag (1958).

26. L.A. Beavan, R.M. Scanlan and D.N. Seidman, Acta Met. 19, 1339 (1971).

27. J.R. Beeler, Jr. in preprints (only) of Vacancies and Interstitials in Metals, Vol. 2 (Zentral bibliothek der Kernforschungsanglage, Jülich GmbH) pp. 598-618. (1968).

28. A. Sosin and H. Neely, Phys. Rev. 127, 1465 (1962).

29. W. Schilling, G. Burger, K. Isebeck and H. Wenzl in Vacancies and Interstitials in Metals, edited by A. Seeger, D. Schumacher, W. Schilling and J. Diehl, pp. 255-361. North-Holland (1970).

30. J.T. Robinson, K.L. Wilson and D.N. Seidman, Phil. Mag. 27, 1417 (1973).

31. D.N. Seidman and K.H. Lie, Acta Met. 20, 1045 (1972).

32. T.T. Tsong, J. Chem. Phys. 55, 4658 (1971).

33. T.T. Tsong and R.J. Walko, Phys. Stat. Sol. (a)12, 111 (1972).

34. M.W. Thompson, Defects and Radiation Damage, pp. 204-214. Cambridge (1969).

35. E.W. Müller and T.T. Tsong, Field Ion Microscopy, Chap. 2. Elsevier (1969).

36. T.J. Wilkes, J.M. Titchmarch, G.D.W. Smith, D.A. Smith, R.F. Morris, S. Johnston, T.J. Godfrey, P. Birdseye, J.Phys. D: Appl. Phys. 5, 2226 (1972).

37. B. Loberg, Phil. Mag. 24, 593 (1971).

Table 1. Chemical composition of the various grades of tungsten and tungsten-rhenium alloys employed.†

Element	Starting Material For Zone-Refining	One-Pass Zone-Refined Tungsten	Four-Pass Zone-Refined Tungsten	Westinghouse Tungsten in The As-Received State	MRC VP Grade Tungsten in The As-Received State	W-0.5 at.% Rhenium	W-3 at.% Rhenium
C	105	*	*	1370	20	*	*
H	*	*	*	*	5	*	*
O	*	*	*	*	25	*	*
N	*	*	*	*	10	*	*
Ag				*	<10		
Al	10-100	0.1-1	1-10	1-10	15	10-100	10-100
As				0.1-1		*	*
Bi	0.3-3			0.1-1		*	*
Ca	10-100	0.1-1	0.1-1		<5	*	*
Co				0.1-1	<10		
Cr	10-100	1-10	0.1-1	10-100	<15		
Cu					<15		
Fe	10-100	1-10			<15	10-100	10-100
K	10-100	0.1-1	0.1-1			10-100	10-100
Mg	6-60	0.1-1	0.1-1		<5		
Mn	<0.3	0.1-1	<0.1		<5		
Mo	1-10			0.1-1	50		
Na		1-10	1-10				
Nb	6-60	0.1-1	0.1-1	*	<15	*	*
P				1-10			
Pb				10-100	<10		
Re		1-10	1-10			10^3-10^4	10^3-10^4
S	0.3-3	*	*	0.1-1		*	*
Si	10-100	10-100	10-100		<10	100-500	100-500
Sn					<10		
Ti	10-100	0.1-1	<0.1	1-10	<10		
V	10-100			1-10			
Zn					<15		

† Concentrations are given in atomic parts per million. The MRC VP grade tungsten composition is the typical analysis provided by MRC. All other measurements were made by the Material Science Center Analytical Laboratory of Cornell University. The carbon concentration was measured by the inert gas fusion technique, while the rest of the analyses were obtained from spark source mass spectroscopy. An asterisk (*) indicates that no analysis was made for that element, or that interferences prohibited its detection.

Table 2. The resistivity ratio (R) for various grades of tungsten used in this experiment.[†]

Type of Specimen	Four-Pass Zone-Refined	One Pass Zone-Refined	Annealed Westinghouse	Materials Research Corp. (MRC) Very Pure (VP) Grade	Westinghouse Tungsten in the As-Received State	Four-Pass Zone-Refined Tungsten Doped with Carbon	Tungsten-0.5 at.% Rhenium	Tungsten-3 at.% Rhenium
R	$3 \cdot 10^4$ to $5 \cdot 10^4$	$1.5 \cdot 10^4$	50	15	5	250	8.7	2.3
Specimen diameter (mm)	1.0	1.0	0.125	0.125	0.125	0.2	0.25	0.13

[†] No corrections have been made for the specimen size effect.

Table 3. A listing of the different types of specimens irradiated, the 30keV W^+ ion dose, the average tip radius and the number of SIA events observed.

Specimen	Dose ($\times 10^{-12}$ ion cm^{-2})	Radius† (Å)	Number of SIA's Observed
Four Pass Zone-Refined Tungsten [R=(3to5)·10^4]			
1*	20.0	250	15
2A	9.5	170	6
2B	13.0	220	17
3A	4.5	325	32
3B	4.0	340	39
4A	5.5	325	84
4B	4.5	380	126
One Pass Zone-Refined Tungsten (R=1.5·10^4)			
1	20.0	230	21
2A	6.6	240	27
2B	5.5	260	35
2C	5.5	275	74
Annealed Westinghouse Tungsten (R=50)			
1A	8.0	300	67
1B	8.0	320	63
1C	6.8	320	82
MRC VP Grade Tungsten (R=15)			
1	25.0	190	12
2	20.0	335	12
3	20.0	250	9
4A	5.6	190	7
4B	20.0	240	7
4C	No measurement	240	5
5	5.4	225	20
6A	5.0	260	45
6B	5.0	300	49
Westinghouse Tungsten In the As-Received State (R=5)			
1	6.0	230	9
2	6.6	285	19
3A	5.5	265	27
3B	7.0	325	28
4	5.8	330	11
5A	5.0	210	16
5B	8.5	292	44
5C	5.7	325	54
Tungsten -0.5 at.% Rhenium (R=8.7)			
1A	3.5	380	17
1B	4.5	380	10
2A	5.0	310	10
2B	6.0	370	25
Tungsten- 3 at.% Rhenium (R=2.3)			
1A	20.0	205	1
1B	50.0	235	1
1C	12.0	235	0
2	20.0	250	1
3A	4.0	315	3
3B	5.0	350	4
Four Pass Zone-Refined Tungsten doped with Carbon (R=250)			
1A	5.2	190	6
1B	4.6	250	20
2A	5.0	185	16
2B	5.0	230	30
2C	5.0	310	72
Annealed Westinghouse Tungsten doped with Carbon			
1	5.0	330	33
2	5.0	280	49
3	5.0	265	15

† Tip radii were measured by the ring counting method of Drechsler and Wolf.[25] An average was taken of the measurements between the 011 and 112 poles.

* The letter A,B and C on the specimen numbers mean that that specimen was re-irradiated (e.g., specimen 2B implies that this was the second irradiation for specimen number 2).

FIGURE CAPTIONS

Fig. 1. A composite isochronal annealing spectrum for one-pass zone-refined tungsten irradiated at 18K with 30keV W^+ ions to a dose of $5 \cdot 10^{12}$ ion cm^{-2} and annealed to 120K at a warming rate of $\sim$2.5K min^{-1}.

Fig. 2. A composite isochronal annealing spectrum for annealed Westinghouse tungsten irradiated at 18K with 30keV W^+ ions to a dose of $5 \cdot 10^{12}$ ion cm^{-2} and annealed to 120K at a warming rate of $\sim$2.5K min^{-1}.

Fig. 3. A composite annealing spectrum for MRC VP grade tungsten irradiated in the as-received state at 18K with 30keV W^+ ions to a dose of $5 \cdot 10^{12}$ ion cm^{-2} and annealed to 120K at a warming rate of $\sim$2.5K min^{-1}.

Fig. 4. Composite isochronal annealing spectra for the four-pass zone-refined, one-pass zone-refined, annealed Westinghouse and MRC VP grade tungsten. A 15K temperature interval was employed; only the data below 87K is included in this analysis.

Fig. 5. A composite isochronal annealing spectrum for Westinghouse tungsten in the as-received state irradiated at 18K with 30keV W^+ ions and annealed to 120K at a warming rate of $\sim$2.5K min^{-1}.

Fig. 6. A composite annealing spectrum for an annealed Westinghouse tungsten specimen with a 2K temperature interval. Only the SIA events detected below 42K are included in this histogram. The analytical expression for an isochronal annealing spectrum based on a diffusion model is superimposed on the experimental results. The specimen was irradiated at 18K with 30keV W^+ ions and warmed at a rate of $\sim$2.5K min^{-1}.

Fig. 7. (A): A composite isochronal annealing spectrum for a tungsten-0.5 at.% rhenium alloy irradiated at 18K with 30keV W^+ ions to a dose of $5 \cdot 10^{12}$ ion cm^{-2} and warmed to 120K at a rate of $\sim$2.5K min^{-1}.

(B): A composite isochronal annealing spectrum for a tungsten-3 at.% rhenium alloy irradiated at 18K with 30keV W^+ ion cm^{-2} and warmed to 120K at a rate of $\sim$2.5K min^{-1}.

Fig. 8. A composite isochronal annealing spectrum for four-pass zone-refined tungsten doped with carbon and irradiated at 18K with 30keV W^+ ions to a dose of $5 \cdot 10^{12}$ ion cm^{-2} and then warmed to 120K at a rate of $\sim$2.5K min^{-1}.

Fig. 9. A composite isochronal annealing spectrum for Westinghouse tungsten doped with carbon and irradiated at 18K with 30keV W^+ ions to a dose of $5 \cdot 10^{12}$ ion cm^{-2} and then warmed to 120K at a rate of $\sim$2.5K min^{-1}.

Fig. 10. The composite isochronal annealing spectra for the two carbon doped tungsten materials. A 15K temperature interval was employed for the analysis and only the date below 87K was included in this analysis.

Fig. 11. (A) and (B): The appearance of a single-spot SIA contrast pattern at 30.5K in the (334) plane during an isochronal anneal.

(C) and (D): The appearance of a single-spot SIA contrast pattern at 36.5K in the (210) plane during an isochronal anneal.

(E) and (F): The appearance of a single-spot SIA contrast pattern at 37.5K in a (110) terrace during an isochronal anneal.

In all cases the micrographs recorded before and after the appearance of the SIA were taken 2.0 sec apart which corresponded to a temperature interval of $\sim$0.08K. The arrow in each pair of micrographs points towards the SIA.

Fig. 12. (A) and (B): The appearance of a double-spot SIA contrast pattern detected in the (110) terraces at 42.0K during an isochronal anneal.

(C) and (D): The appearance of another double-spot SIA contrast pattern in the (110) terraces at 54.0K during an isochronal anneal.

(E) and (F): The appearance of a multiple-spot SIA contrast pattern near the (210) plane at 50.0K during an isochronal anneal.

(G) and (H): The appearance of a multiple-spot SIA contrast pattern near the (112) plane at 64.5K during an isochronal anneal. The entire surface is seen to change dramatically in this region for this particular event.

In all four cases the micrographs recorded before and after the appearance of the SIA were taken 2.0 sec apart, which corresponds to a temperature interval of $\sim$0.08K.

Fig. 13. A composite isochronal annealing spectrum for double-spot SIA contrast patterns from all five grades of unalloyed and undoped tungsten.

Fig. 14. A composite isochronal annealing spectrum for annealed Westinghouse tungsten irradiated with 30keV W^+ ions at 18K to a dose of $5 \cdot 10^{13}$ ion cm^{-2}.

Fig. 15. The appearance of a defect found during pulse field evaporation of an MRC tungsten crystal irradiated at 18K, warmed to 120K, and recooled to 18K. Frame 1 shows a normal (334) layer. Frames 47 and 91 show the next two layers, in which vacant sites (0) were observed. Frames 135-183 show the pulse field evaporation of layer 4. Frame 135 shows a high degree of strain in the layer. In frame 136, an "extra bright spot" (denoted by ⊛) is seen to appear. This "extra bright spot" and two neighboring atoms are preferentially retained on the surface until frame 190. This last frame in the sequence shows layer 5, with two vacant sites visible.

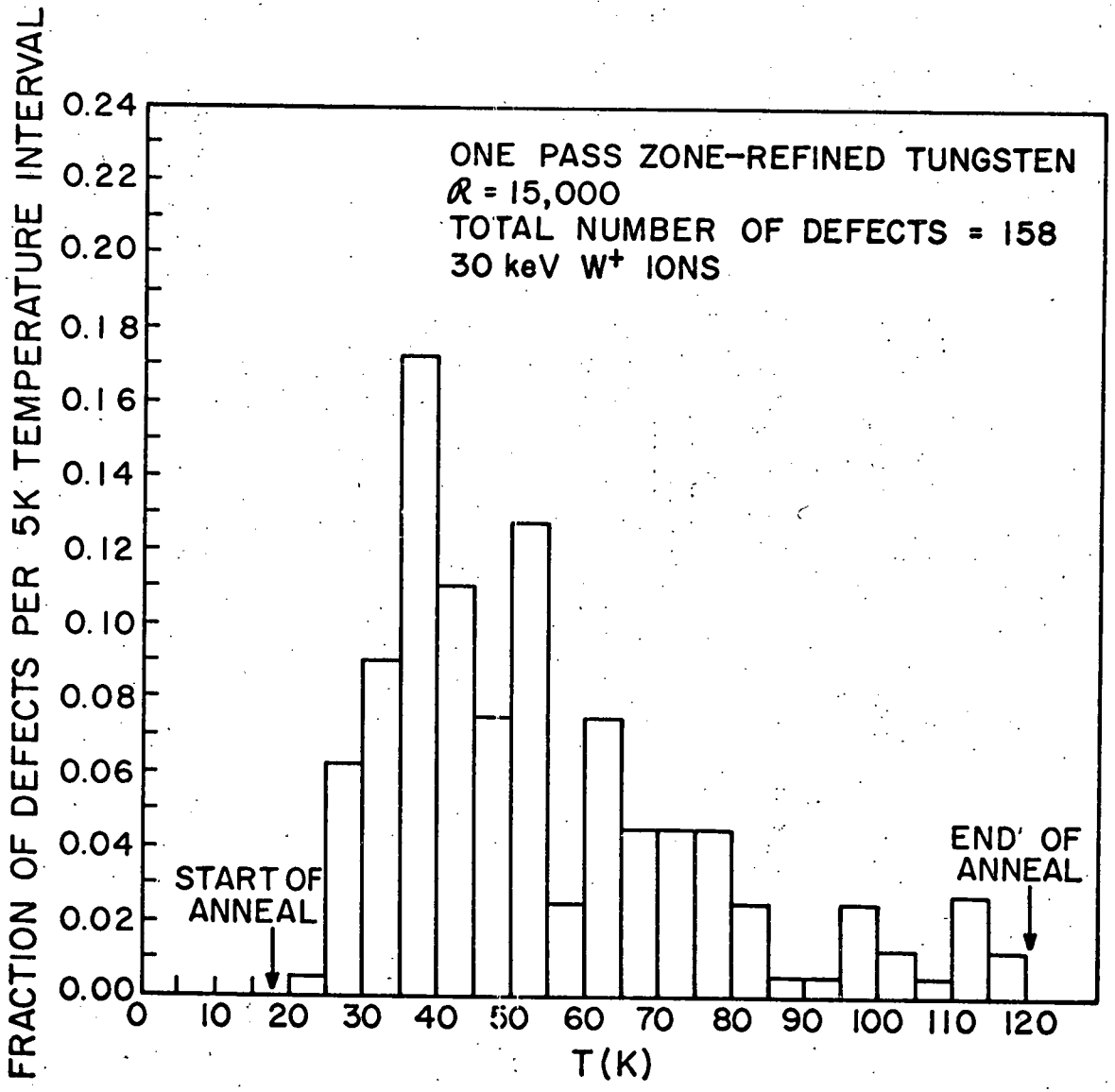
ONE PASS ZONE-REFINED TUNGSTEN
R = 15,000
TOTAL NUMBER OF DEFECTS = 158
30 keV W+ IONS
FRACTION OF DEFECTS PER 5K TEMPERATURE INTERVAL
0.24
0.22
0.20
0.18
0.16
0.14
0.12
0.10
0.08
0.06
0.04
0.02
0.00
START OF ANNEAL
END OF ANNEAL
0
10
20
30
40
50
60
70
80
90
100
110
120
T(K)

Figure 1

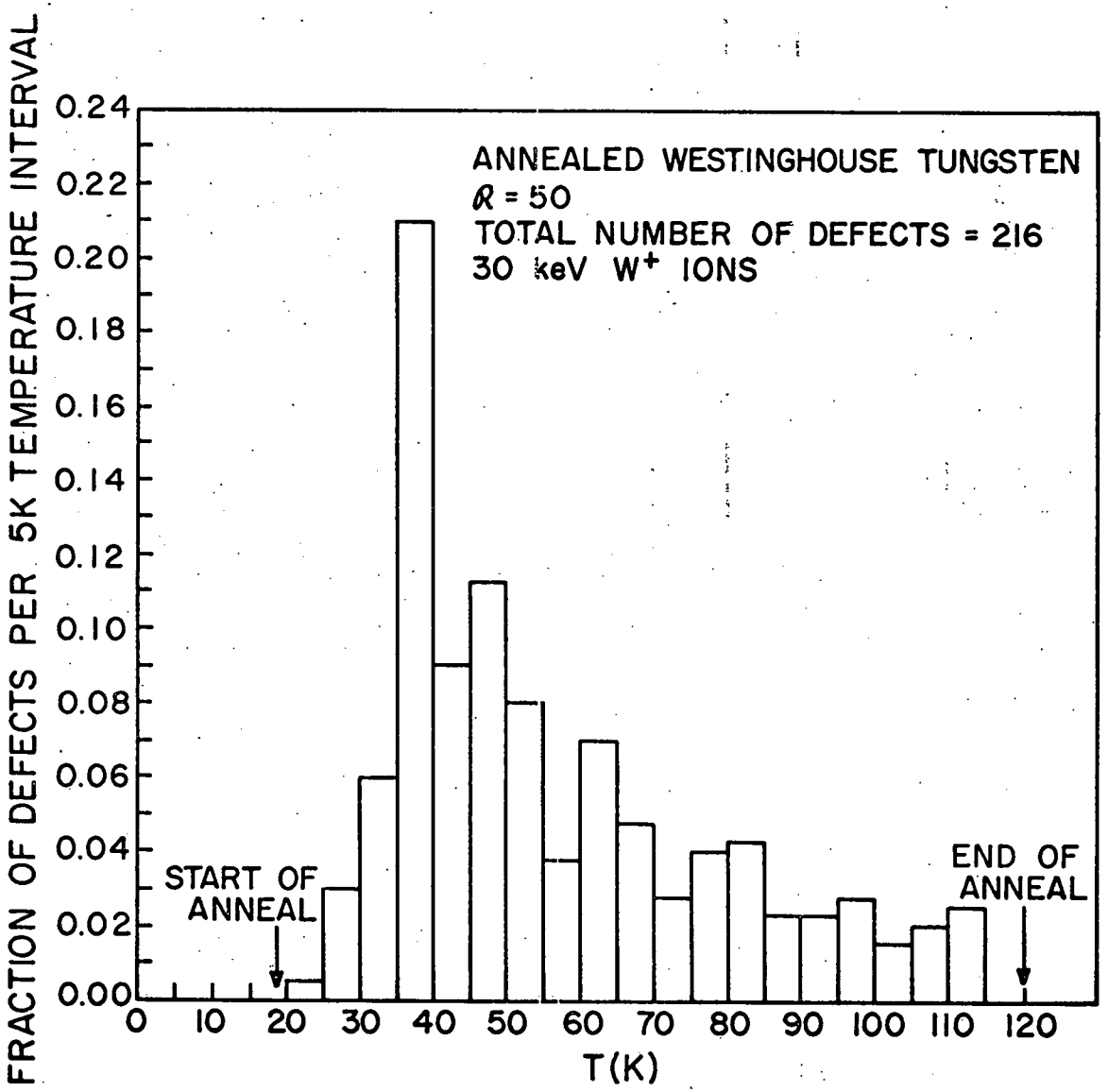
ANNEALED WESTINGHOUSE TUNGSTEN
R = 50
TOTAL NUMBER OF DEFECTS = 216
30 keV W+ IONS
START OF ANNEAL
END OF ANNEAL
FRACTION OF DEFECTS PER 5K TEMPERATURE INTERVAL
0.24
0.22
0.20
0.18
0.16
0.14
0.12
0.10
0.08
0.06
0.04
0.02
0.00
0 10 20 30 40 50 60 70 80 90 100 110 120
T(K)

Figure 2

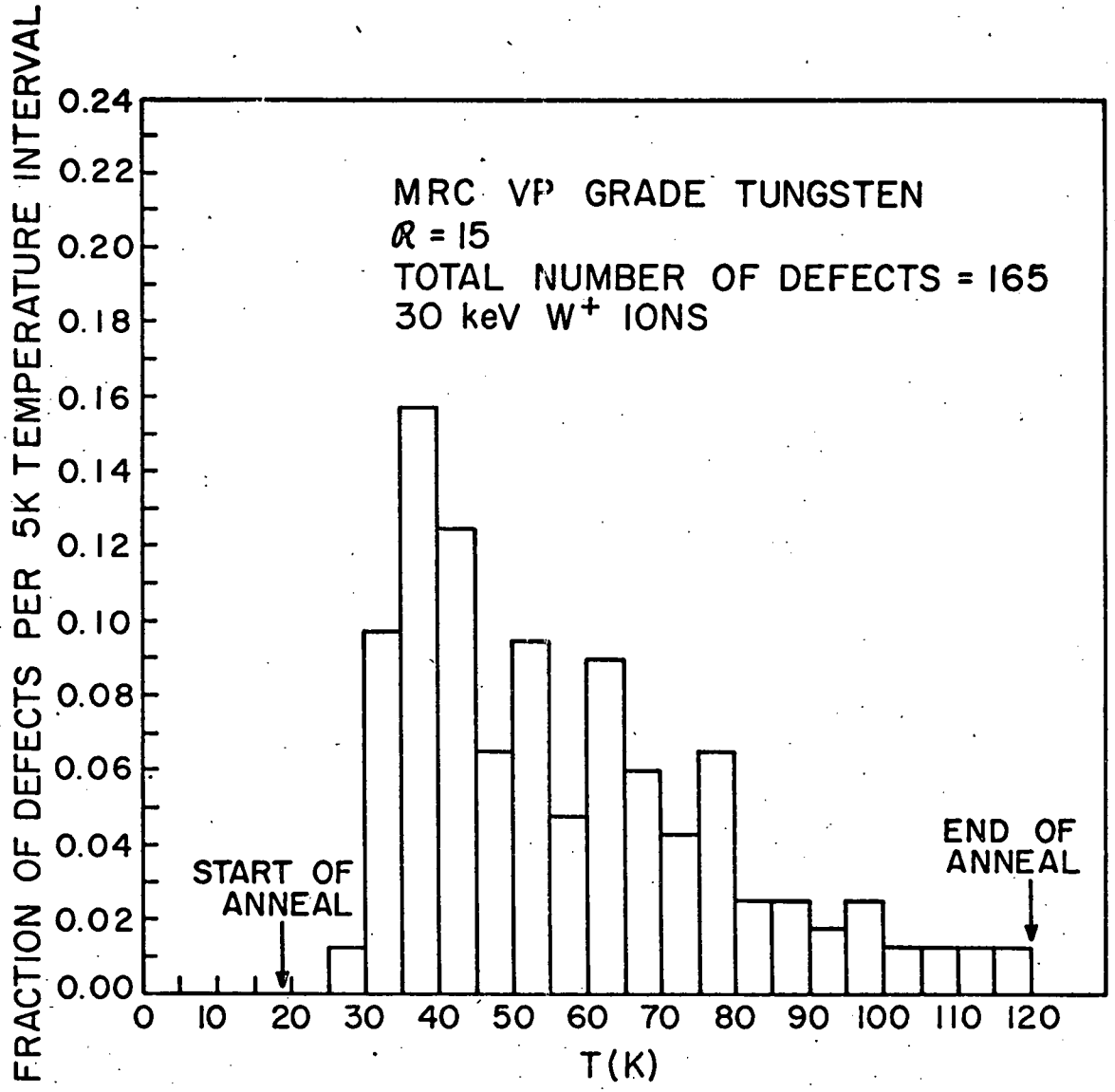
FRACTION OF DEFECTS PER 5K TEMPERATURE INTERVAL
0.24
0.22
0.20
0.18
0.16
0.14
0.12
0.10
0.08
0.06
0.04
0.02
0.00
MRC VP GRADE TUNGSTEN
R = 15
TOTAL NUMBER OF DEFECTS = 165
30 keV W+ IONS
START OF ANNEAL
END OF ANNEAL
0 10 20 30 40 50 60 70 80 90 100 110 120
T(K)

Figure 3

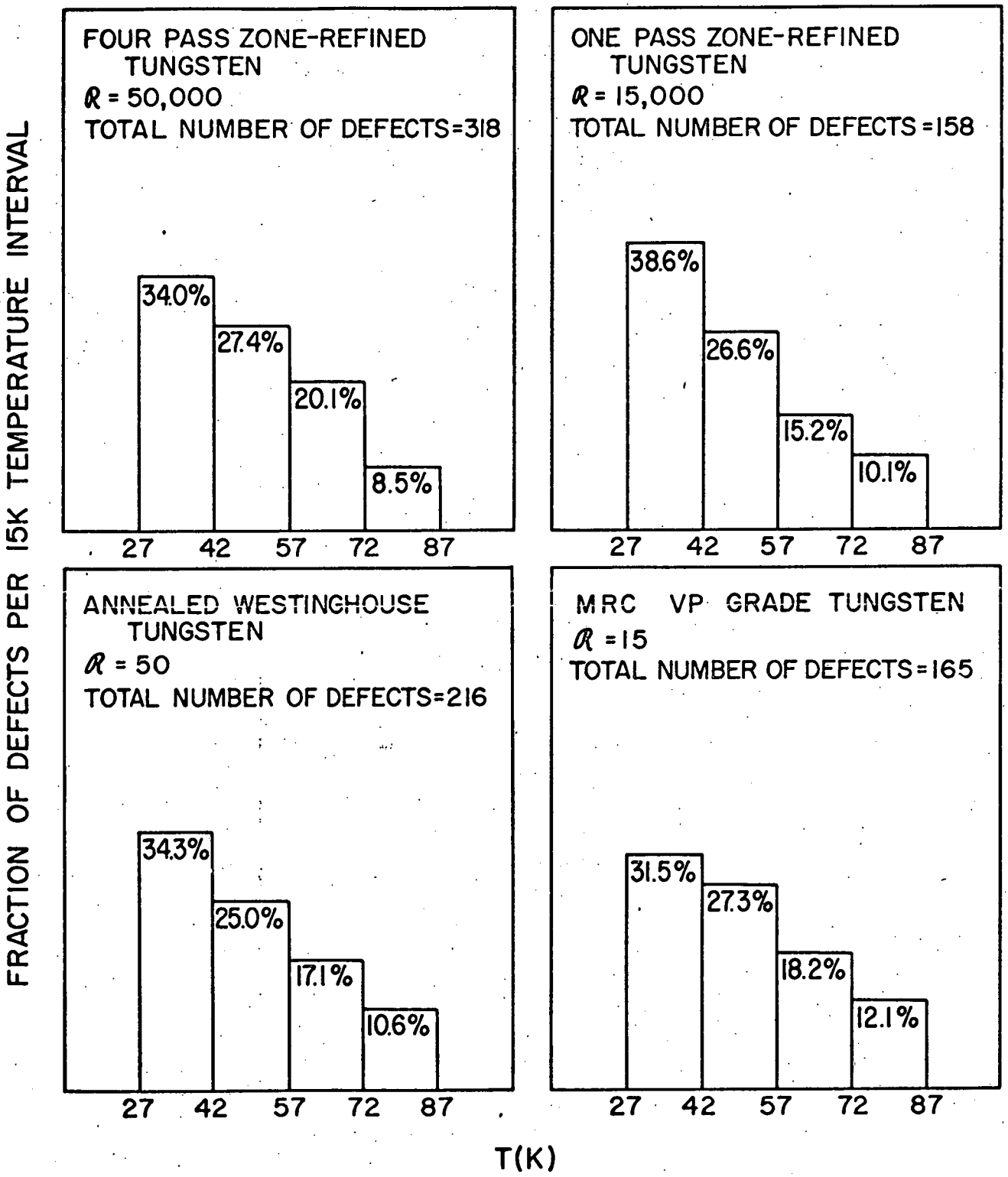
FOUR PASS ZONE-REFINED TUNGSTEN
R = 50,000
TOTAL NUMBER OF DEFECTS=318
34.0%
27.4%
20.1%
8.5%
27 42 57 72 87
ONE PASS ZONE-REFINED TUNGSTEN
R = 15,000
TOTAL NUMBER OF DEFECTS=158
38.6%
26.6%
15.2%
10.1%
27 42 57 72 87
ANNEALED WESTINGHOUSE TUNGSTEN
R = 50
TOTAL NUMBER OF DEFECTS=216
34.3%
25.0%
17.1%
10.6%
27 42 57 72 87
MRC VP GRADE TUNGSTEN
R = 15
TOTAL NUMBER OF DEFECTS=165
31.5%
27.3%
18.2%
12.1%
27 42 57 72 87
FRACTION OF DEFECTS PER 15K TEMPERATURE INTERVAL
T(K)

Figure 4

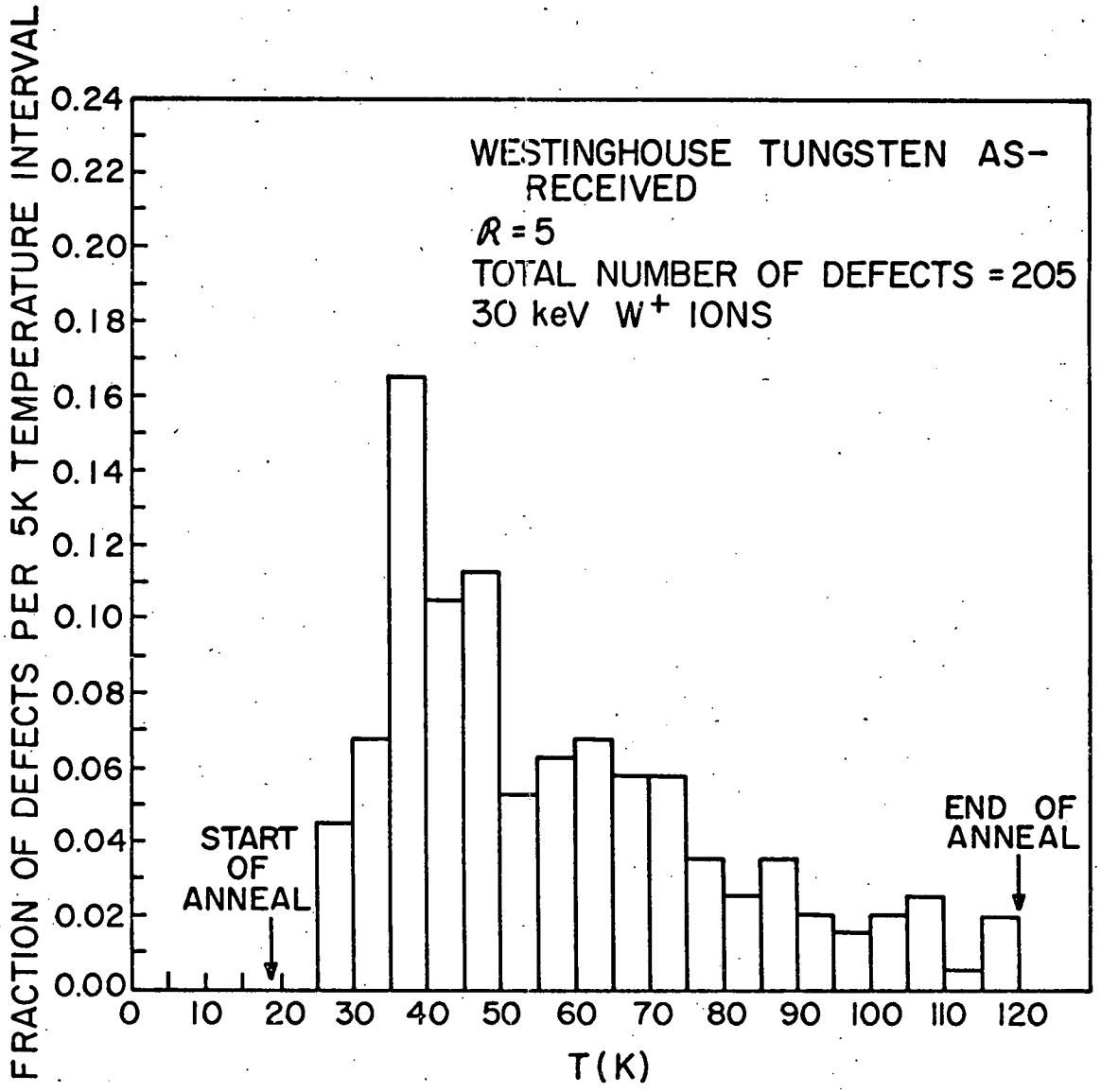
WESTINGHOUSE TUNGSTEN AS-RECEIVED
R = 5
TOTAL NUMBER OF DEFECTS = 205
30 keV W+ IONS
START OF ANNEAL
END OF ANNEAL
FRACTION OF DEFECTS PER 5K TEMPERATURE INTERVAL
0.24
0.22
0.20
0.18
0.16
0.14
0.12
0.10
0.08
0.06
0.04
0.02
0.00
0
10
20
30
40
50
60
70
80
90
100
110
120
T(K)

Figure 5

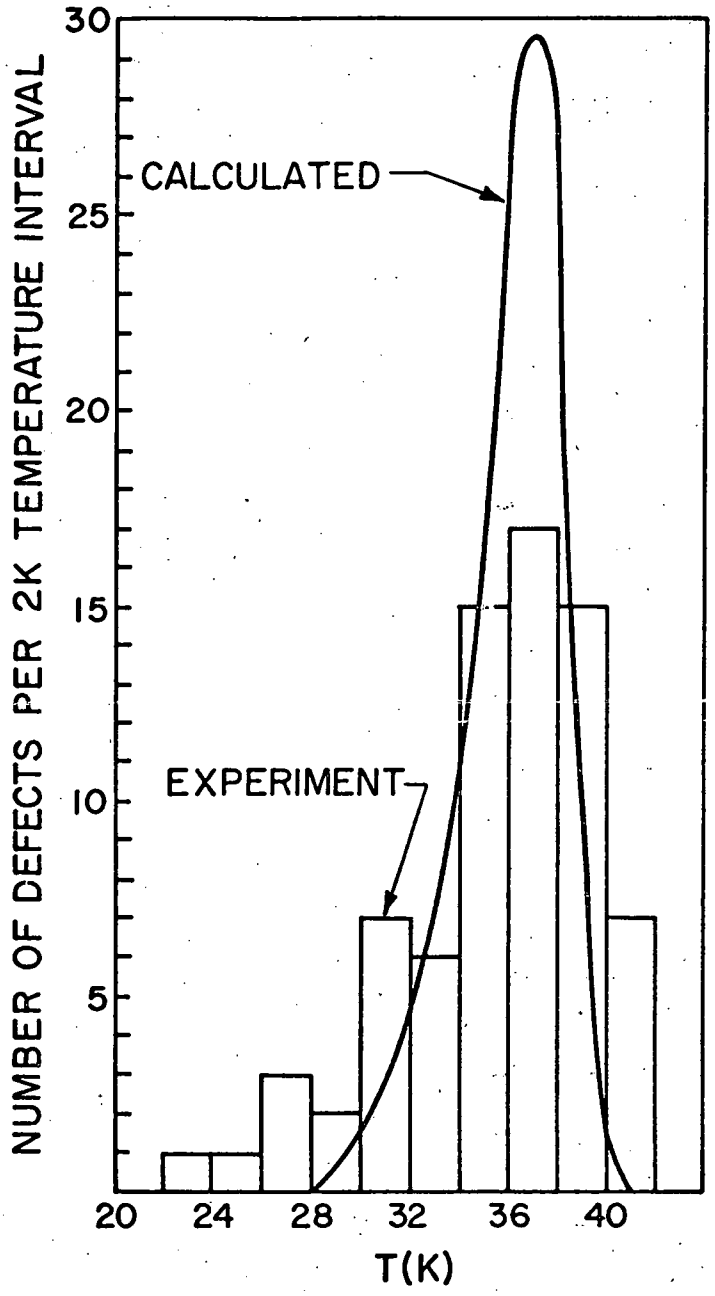
NUMBER OF DEFECTS PER 2K TEMPERATURE INTERVAL
30
25
20
15
10
5
CALCULATED
EXPERIMENT
20
24
28
32
36
40
T(K)

Figure 6

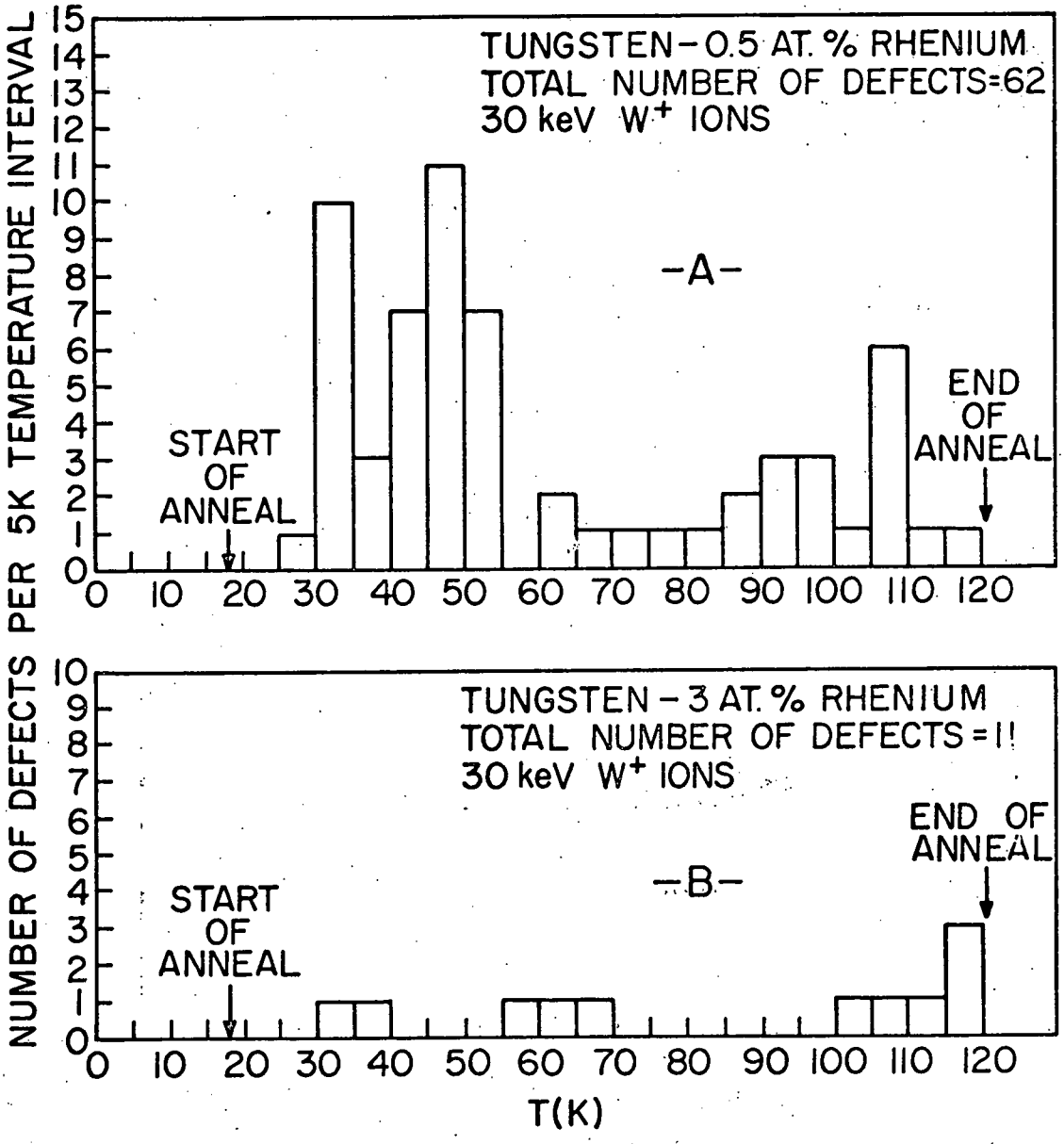
TUNGSTEN – 0.5 AT. % RHENIUM
TOTAL NUMBER OF DEFECTS=62
30 keV W+ IONS
-A-
START OF ANNEAL
END OF ANNEAL
TUNGSTEN – 3 AT. % RHENIUM
TOTAL NUMBER OF DEFECTS = 11
30 keV W+ IONS
-B-
START OF ANNEAL
END OF ANNEAL
NUMBER OF DEFECTS PER 5K TEMPERATURE INTERVAL
T(K)

Figure 7

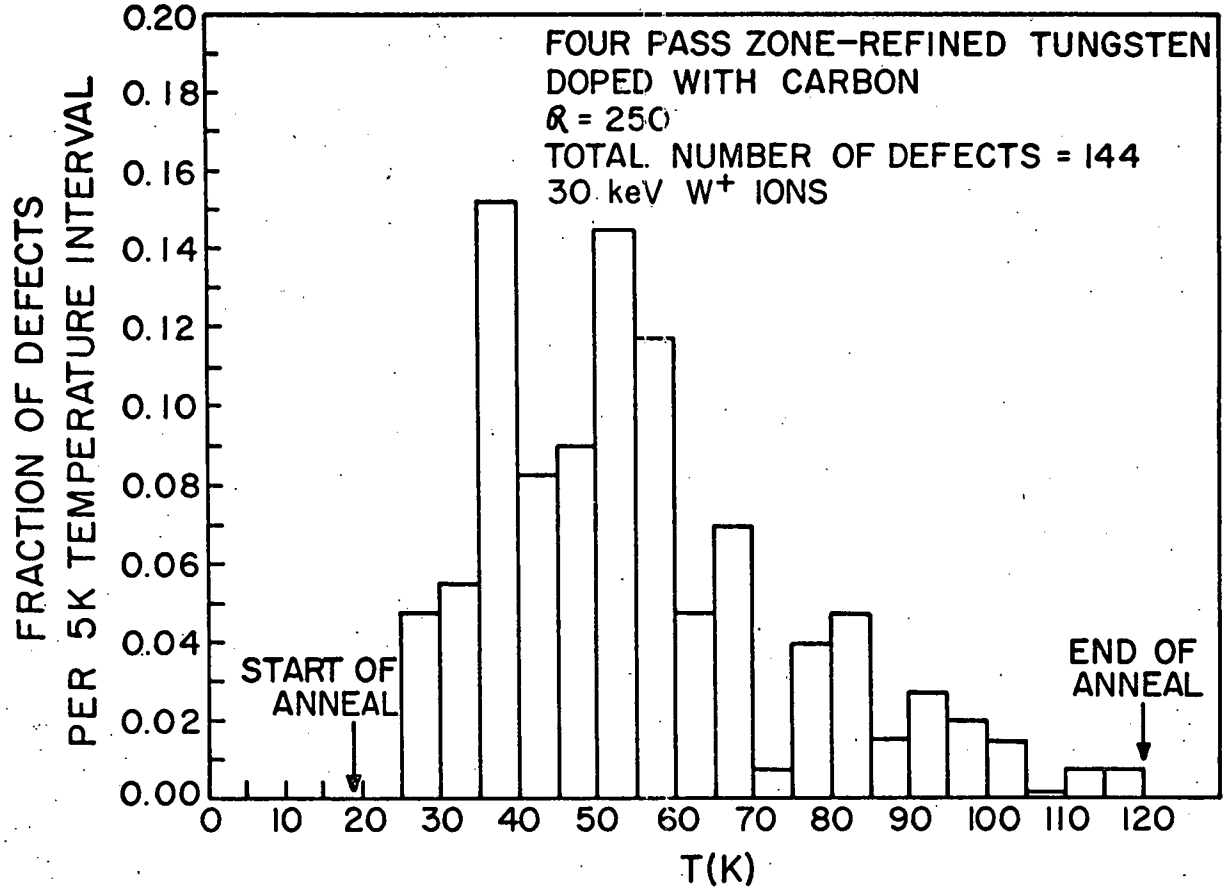
FOUR PASS ZONE-REFINED TUNGSTEN
DOPED WITH CARBON
R = 250
TOTAL. NUMBER OF DEFECTS = 144
30 keV W+ IONS
FRACTION OF DEFECTS
PER 5K TEMPERATURE INTERVAL
0.20
0.18
0.16
0.14
0.12
0.10
0.08
0.06
0.04
0.02
0.00
START OF
ANNEAL
END OF
ANNEAL
0
10
20
30
40
50
60
70
80
90
100
110
120
T(K)

Figure 8

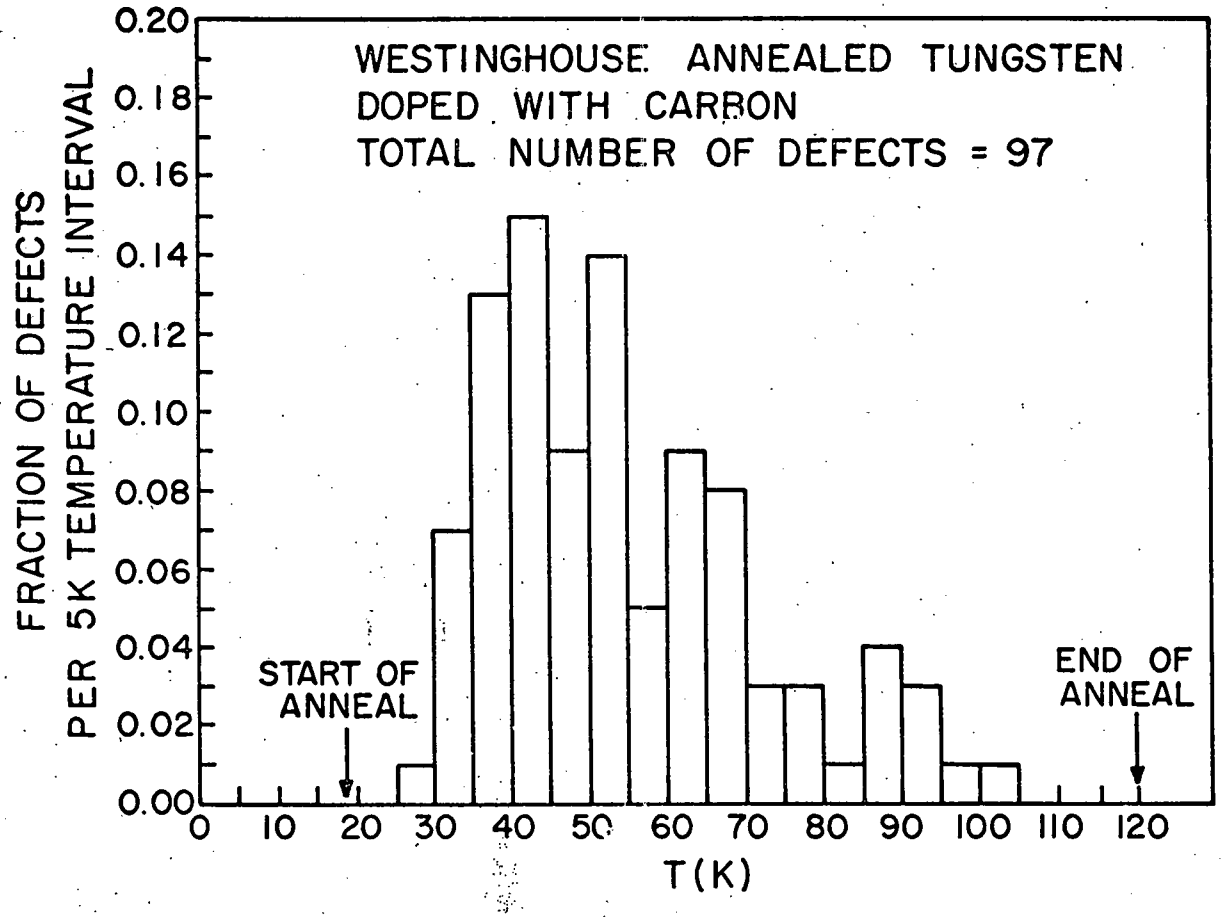
WESTINGHOUSE ANNEALED TUNGSTEN
DOPED WITH CARBON
TOTAL NUMBER OF DEFECTS = 97
FRACTION OF DEFECTS
PER 5K TEMPERATURE INTERVAL
0.20
0.18
0.16
0.14
0.12
0.10
0.08
0.06
0.04
0.02
0.00
START OF
ANNEAL
END OF
ANNEAL
0
10
20
30
40
50
60
70
80
90
100
110
120
T(K)

Figure 9

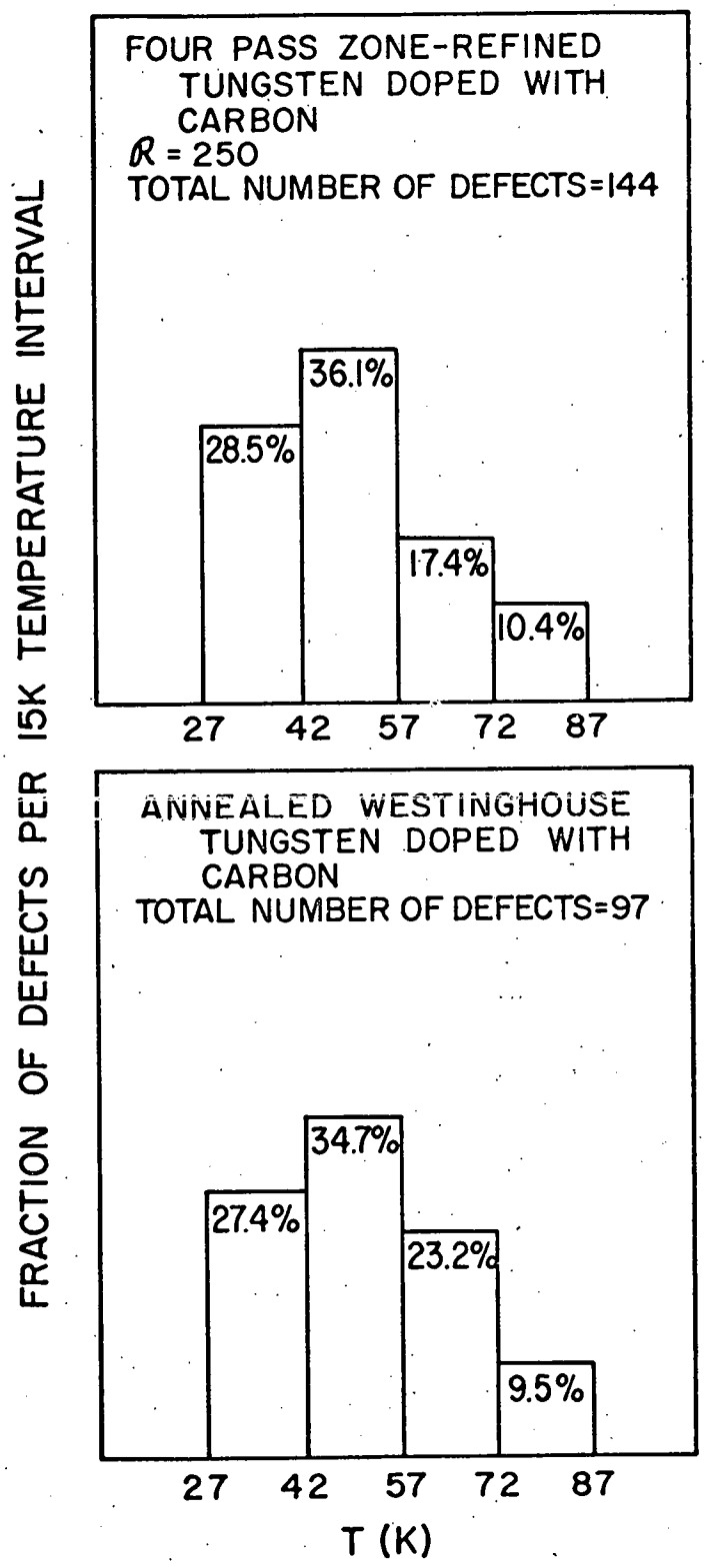
FOUR PASS ZONE-REFINED
TUNGSTEN DOPED WITH
CARBON
R = 250
TOTAL NUMBER OF DEFECTS=144
28.5%
36.1%
17.4%
10.4%
27
42
57
72
87
ANNEALED WESTINGHOUSE
TUNGSTEN DOPED WITH
CARBON
TOTAL NUMBER OF DEFECTS=97
27.4%
34.7%
23.2%
9.5%
27
42
57
72
87
T (K)
FRACTION OF DEFECTS PER 15K TEMPERATURE INTERVAL

Figure 10

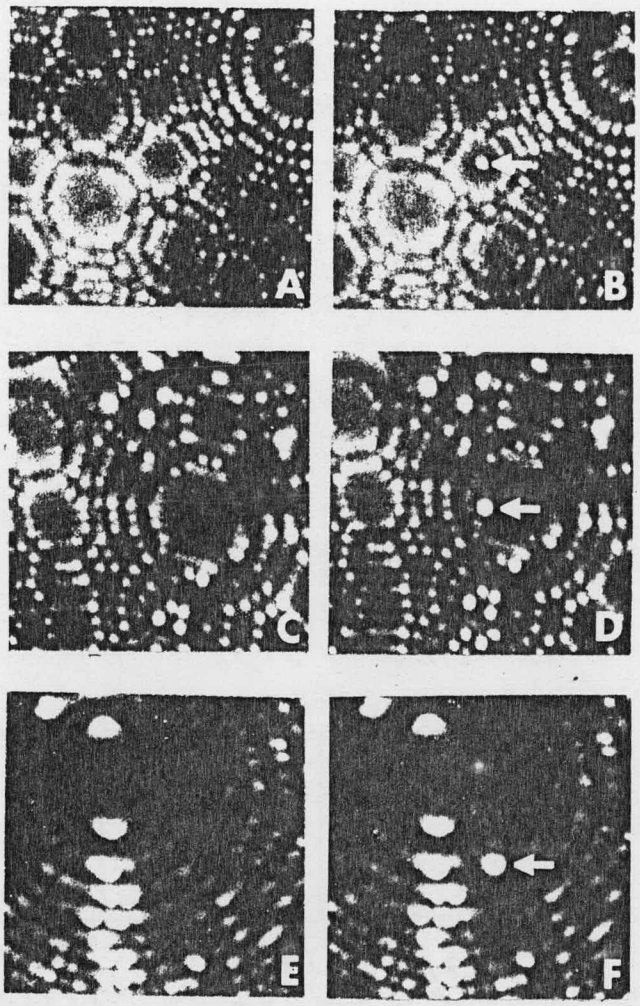

Figure 11

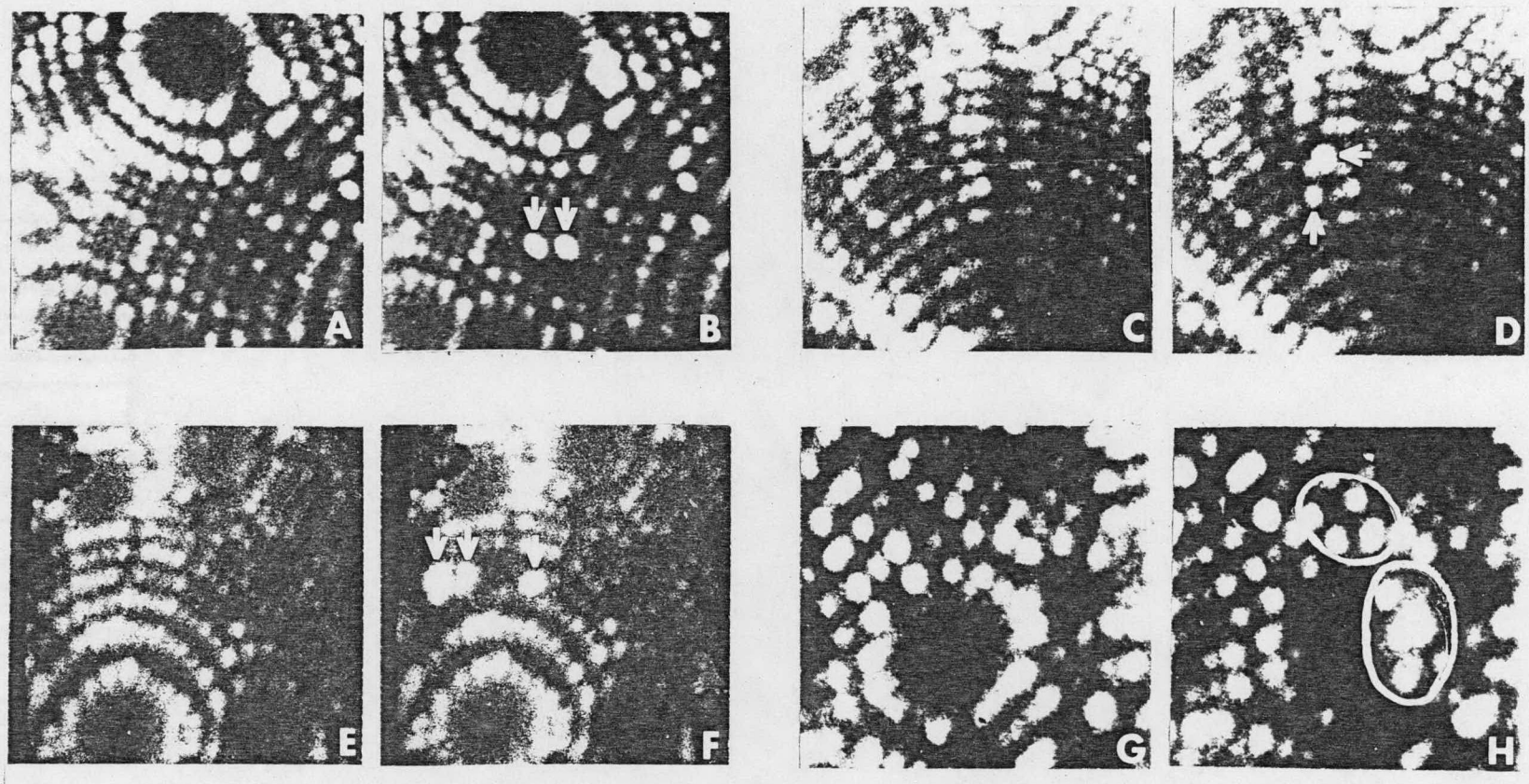

Figure 12

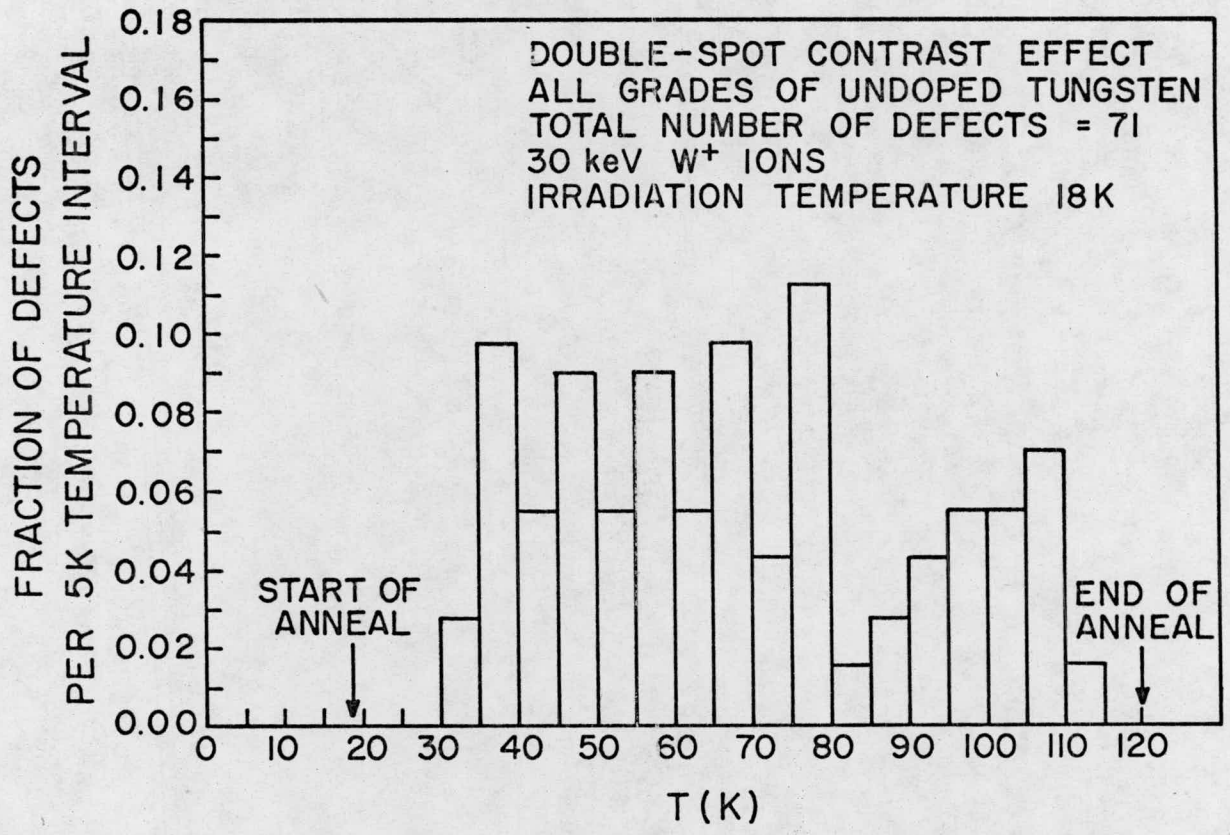
DOUBLE-SPOT CONTRAST EFFECT
ALL GRADES OF UNDOPED TUNGSTEN
TOTAL NUMBER OF DEFECTS = 71
30 keV W+ IONS
IRRADIATION TEMPERATURE 18K
FRACTION OF DEFECTS
PER 5K TEMPERATURE INTERVAL
0.18
0.16
0.14
0.12
0.10
0.08
0.06
0.04
0.02
0.00
START OF
ANNEAL
END OF
ANNEAL
0
10
20
30
40
50
60
70
80
90
100
110
120
T(K)

Figure 13

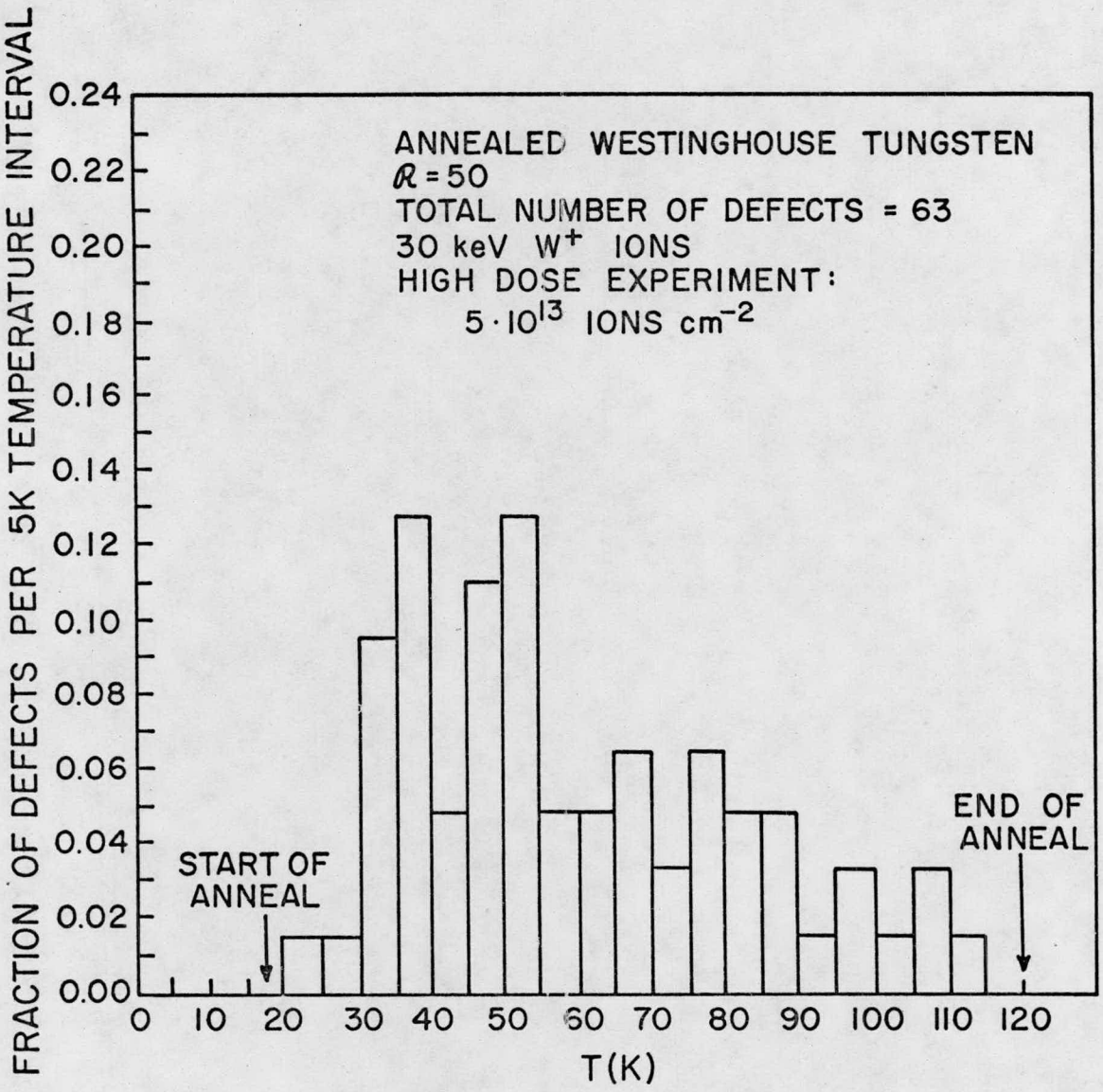
ANNEALED WESTINGHOUSE TUNGSTEN
R = 50
TOTAL NUMBER OF DEFECTS = 63
30 keV W+ IONS
HIGH DOSE EXPERIMENT:
5·10^13 IONS cm^-2
START OF ANNEAL
END OF ANNEAL
FRACTION OF DEFECTS PER 5K TEMPERATURE INTERVAL
0.24
0.22
0.20
0.18
0.16
0.14
0.12
0.10
0.08
0.06
0.04
0.02
0.00
0 10 20 30 40 50 60 70 80 90 100 110 120
T(K)

Figure 14

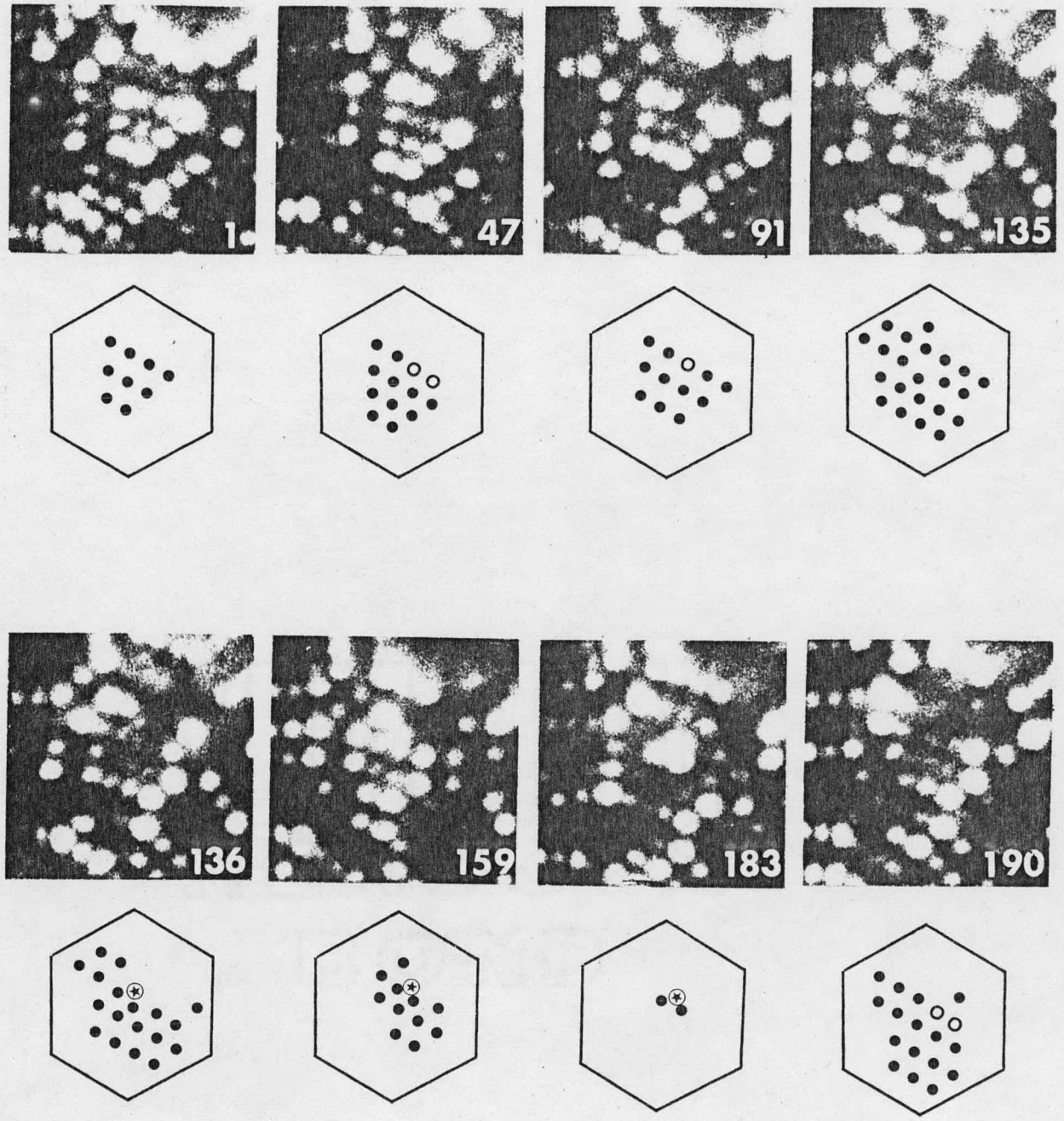

Figure 15